Quantum Hall response of SU(3) fermions

Man Hon Yau and C. A. R. Sá de Melo
School of Physics, Georgia Institute of Technology, Atlanta, Georgia 30332, USA

(Received 28 June 2022; accepted 17 October 2022; published 16 November 2022)

We discuss the quantum Hall response of SU(3) fermions in two-dimensional lattices, when artificial magnetic flux and color-orbit coupling are present. We analyze the Hall conductance tensor in the charge-charge, color-charge, charge-color, and color-color sectors. When charge and color are conserved, we directly relate the Hall conductances to corresponding Chern numbers describing topological color insulators. We establish the bulk-edge correspondence for Hall conductances in toroidal (without edges) and cylindrical (with edges) geometries. When color is not conserved or when edge states are not robust to disorder or SU(3)-symmetric interactions, we show that the color Hall conductances are not quantized, but the corresponding Chern numbers, which are a bulk property, can still be used to label the topological insulating phases. Depending on the robustness of edge states to disorder and interactions, we identify the topological phases to be *strong*, *intermediate*, or *weak*. We envision applications to SU(N) ultracold fermions such as ^{173}Yb and ^{87}Sr.

DOI: 10.1103/PhysRevA.106.053313

I. INTRODUCTION

It is now well established that SU(N) fermions with three internal states ($N = 3$) or more can be loaded into optical lattices. Examples of such experimental systems are ^{173}Yb [1–9], with $N \leqslant 6$, and ^{87}Sr [10–13], with $N \leqslant 10$, which have SU(N) symmetric interactions. Some experiments with SU(2) spin-1/2 neutral fermions in two-dimensional optical lattices simulated Harper-Hofstadter Hamiltonians for fictitious magnetic fields [14,15], and others explored topological properties such as Chern numbers [16,17] based on theoretical suggestions [18–20]. These experiments were largely inspired by the desire to simulate known effects found in condensed-matter physics such as the quantization of the Hall conductance in large magnetic fields [21–24], quantum Hall effect in the absence of Landau levels [25], or the quantum spin-Hall effect with spin-orbit coupling [26–28]. However, corresponding experimental generalizations to study SU(3) fermions in the presence of fictitious magnetic fields and color-orbit coupling have not yet been implemented. Thus, very little is experimentally known about the topological properties of neutral SU($N \geqslant 3$) fermions and their insulating phases.

In this paper, we discuss the quantum Hall response of SU(3) fermions in two-dimensional optical lattices, when artificial magnetic, color-orbit, and color-flip fields are present. This paper is the extension of our previous work [29,30], where the concept of topological color insulators was introduced, and contains several additional results discussed below. The first additional result is a concrete experimental proposal to measure the quantum Hall responses of SU(3) fermions, including the color-color Hall conductance. The second additional result is the establishment of the connection between the quantum Hall conductances and the Chern matrix when color projection is not conserved. We emphasize that in [29,30], only the connection to the conserved case was made. The third additional result is the derivation of Kubo formulas for the quantum Hall conductances including the case of nonconserved color projection, where additional contributions containing color torques emerge. We point out that in [29,30], there is no discussion about color torques. The fourth additional result is that quantum Hall conductances may no longer be quantized when color torques exist and, thus, may not be directly related to Chern numbers, which can still be used to classify topological phases. We note that in [29,30], this situation was not discussed. The fifth additional result is the derivation of the color continuity equation including color-torque terms, and the establishment of the bulk-edge correspondence in the presence of color torques. We mention that this is not derived in [29,30]. The sixth additional result is an analysis of the magnetization of edge states, a topic that was not mentioned in [29,30]. The seventh additional result is a detailed discussion of the robustness of edge states to weak, local, static, and color-dependent or color-independent disorder which was not analyzed in [29] and was briefly mentioned (one sentence) in [30]. The eighth additional result is a thorough investigation of the effects of local SU(3) interactions on edge states. For clarity, specific examples of topological phases with a few edge states are presented. This was not discussed in [29] and only briefly mentioned in [30]. The ninth additional result is the discovery of intermediate topological phases in addition to the typical weak and strong ones, found in standard SU(2) spin-1/2 topological insulators. This finding provides a refined classification of topological insulators in SU(3) systems. Such result was not described in [29,30].

Although we focus on ultracold fermions with three internal states with assigned colors $\{R, G, B\}$ or pseudospins $\{\uparrow, 0, \downarrow\}$, the generalization to SU(N) fermions is straightforward and can be applied to the full SU(6) symmetry of ^{173}Yb or the full SU(10) symmetry of ^{87}Sr. We concentrate on the SU(3) case because it already shows highly nontrivial generalizations with respect to the standard SU(2) spin-1/2 case of condensed-matter physics.

 ©2022 American Physical Society

The remainder of this paper is organized as follows. In Sec. II, we discuss the experimental setup for a two-dimensional optical lattice and the engineering of a Hamiltonian with artificial magnetic, color-orbit, and color-flip fields, where the quantum Hall response of SU(3) fermions can be investigated. In Sec. III, we give expressions for the Hall conductances in terms of response functions associated with charge and color currents and highlight the emergence of color-torque terms, when color is not conserved. In Sec. IV, we describe the Chern matrix and define three topological invariants that characterize the insulating states of SU(3) fermions: the charge-charge Chern number $\mathcal{C}^{\rm chch}$, the color-charge Chern number $\mathcal{C}^{\rm coch}$ or charge-color Chern number $\mathcal{C}^{\rm chco}$, and the color-color Chern number $\mathcal{C}^{\rm coco}$. In Sec. V, we relate the Hall conductances to their appropriate Chern numbers when charge and color are conserved. We also show that when color is not conserved, the color Hall conductances are not directly proportional to Chern numbers, and thus not quantized. Nevertheless, the Chern numbers can still be used to classify the topological phases, since they are bulk properties of the ground state. In Sec. VI, we discuss the bulk-edge correspondence for SU(3) fermions for the Hall conductances using toroidal boundary conditions with no edges versus cylindrical boundary conditions with two edges. In Sec. VII, we investigate a few examples of edge states, their wave functions, and magnetizations, which set the stage for understanding the robustness of edge states against disorder and SU(3)-symmetric interactions, which is analyzed in Sec. VIII. In Sec. IX, we highlight the classification of topological color insulators based on three Chern numbers, and refine this classification into *strong*, *intermediate*, or *weak* topological color insulators depending on the robustness of edge states with respect to disorder or interactions. In Sec. X, we present our conclusions and share one important outlook regarding the bulk measurements of color Chern numbers, when color Hall conductances are not quantized.

II. ENVISIONED EXPERIMENTAL SETUP

We envision an experimental setup for a two-dimensional lattice in the xy plane with lattice spacing a_x (a_y), and finite extent L_x (L_y) along the x (y) direction, as illustrated schematically in Fig. 1. We imagine an artificial magnetic field H_z applied perpendicularly to the plane, that is, along the z direction, producing an artificial vector potential $\mathcal{A}_y = eH_z x/\hbar c$ represented by the gauge field $\theta_y = \mathcal{A}_y \eta_y I$, where I is the 3×3 identity matrix and $\eta_y = \pm a_y$ are displacements along the y direction. Such artificial lattice gauge field θ_y can be realized experimentally via laser assisted tunneling [14,15] and produces an artificial magnetic flux $\Phi = H_z a_x a_y$ in the lattice plaquette. For these types of systems, the Hall response is directly associated to the charge-charge conductance, and Chern numbers were extracted from measurements in SU(2) spin-1/2 ultracold fermions [16,17]. However, we would like to explore further a situation where color-orbit coupling is introduced, in analogy with spin-orbit coupling when only two internal states are involved, where either Raman processes [31] or radio-frequency chips [32] are responsible for the effect. We illustrate the simplest case of color-orbit coupling k_T and color-flip fields h_x, where the color-dependent momentum

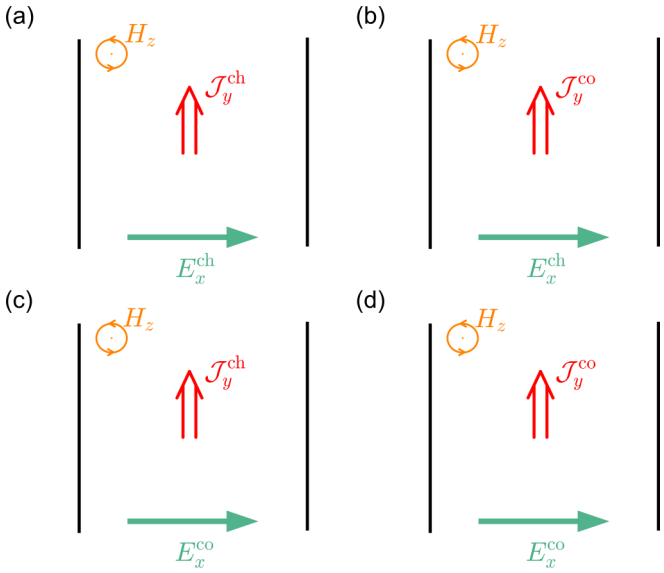

FIG. 1. Schematic drawings of the experimental setup showing the fictitious magnetic field H_z, charge and color electric fields, as well as charge and color Hall currents. (a) The charge electric field $E_x^{\rm ch}$ along x, and the charge Hall current density $\mathcal{J}_y^{\rm ch}$ along y. (b) The charge electric field $E_x^{\rm ch}$ along x, and color Hall current density $\mathcal{J}_y^{\rm co}$ along y. (c) The color electric field $E_x^{\rm co}$ along x, and charge Hall current density $\mathcal{J}_y^{\rm ch}$ along y. (d) The color electric field $E_x^{\rm co}$ along x, and color Hall current density $\mathcal{J}_y^{\rm co}$ along y.

transfer occurs only along the x direction and h_x only flip states $R \to G$ and $G \to B$ and vice versa. The artificial color-orbit coupling k_T is described by a color-dependent gauge field $\theta_x = k_T \eta_x J_z$, where J_z is the spin-1 matrix along z, and $\eta_x = \pm a_x$ is a displacement along x, while h_x plays the role of a Zeeman field along x.

For deep optical lattice potentials, this experimental setup results in two-dimensional lattices with tight-binding Hamiltonian

$$\hat{H} = -\sum_{\mathbf{r},\boldsymbol{\eta}_\ell} t_\ell \mathbf{\Phi}^\dagger(\mathbf{r}) e^{-i\theta_\ell} \mathbf{\Phi}(\mathbf{r}+\boldsymbol{\eta}_\ell) - h_x \sum_{\mathbf{r}} \mathbf{\Phi}^\dagger(\mathbf{r}) J_x \mathbf{\Phi}(\mathbf{r}), \tag{1}$$

where t_ℓ are hopping energies along the $\ell = \{x, y\}$ direction, while θ_ℓ are the gauge fields and h_x is the color-flip field defined above. The fermion creation operators are three-component vectors $\mathbf{\Phi}^\dagger(\mathbf{r}) = [\phi_R^\dagger(\mathbf{r}), \phi_G^\dagger(\mathbf{r}), \phi_B^\dagger(\mathbf{r})]$ with color $c = \{R, G, B\}$, where $\mathbf{r} = (x, y)$ is the position in the lattice. The nearest-neighbor position $\mathbf{r} + \boldsymbol{\eta}_\ell$ with respect to $\mathbf{r}$ is identified with the help of the vectors $\boldsymbol{\eta}_\ell = \eta_\ell \hat{\boldsymbol{\ell}}$, with $\eta_x = \pm a_x$ and $\eta_y = \pm a_y$ defined earlier.

The central idea is to apply either an artificial charge electric field $E_x^{\rm ch}$ or an artificial color electric field $E_x^{\rm co}$ along x and detect charge currents densities $\mathcal{J}_y^{\rm ch}$ or color current densities $\mathcal{J}_y^{\rm co}$ along y, in analogy with the more familiar SU(2) case when charge and spin 1/2 are involved [33,34]. The artificial charge electric field $E_x^{\rm ch}$ is obtained from potential-energy operator $\hat{U}_x^{\rm ch} = -E_x^{\rm ch} ex I$, and can be viewed as an *electrochemical* tilt to the lattice along the x direction, that is a spatially dependent chemical potential

$\mu(x)$. The artificial color electric field $E_x^{\rm co}$ along x is obtained from the potential-energy operator $\hat{U}_x^{\rm co} = -E_x^{\rm co}\hbar x J_\ell$, where ℓ represents a chosen quantization axis. In a more familiar language $\hat{U}_x^{\rm co} = -h_\ell(x)J_\ell$, where $h_\ell(x) = E_x^{\rm co}\hbar x$ is a spatially dependent Zeeman field, leading to the Zeeman force $F_x^{\rm co} = -\partial h_\ell(x)/\partial x = \hbar E_x^{\rm co}$. These are magnetic (color) forces that act on the spin (color) states in a Stern-Gerlach configuration for a spin-1 (color) system. Notice that the color and charge fields defined do not have the same units; this is also reflected in the Hall conductances and the charge- and color-current responses. We will return to this point when discussing the connection between Hall conductances and Chern numbers in Sec. V and the comparison to SU(2) spin-1/2 systems.

For the experimental setup of Fig. 1, the current densities are

$$\begin{pmatrix} \mathcal{J}_y^{\rm ch} \\ \mathcal{J}_y^{\rm co} \end{pmatrix} = \begin{pmatrix} \sigma_{yx}^{\rm chch} & \sigma_{yx}^{\rm chco} \\ \sigma_{yx}^{\rm coch} & \sigma_{yx}^{\rm coco} \end{pmatrix} \begin{pmatrix} E_x^{\rm ch} \\ E_x^{\rm co} \end{pmatrix} \tag{2}$$

where $\sigma_{yx}^{\lambda\tau}$ are the generalized Hall conductances, with λ and τ referring to $\{\rm ch, co\}$. The directions of the charge and color electric fields as well as of the charge and color current responses are illustrated in Fig. 1. We note that there are four types of responses, that is, the production of charge or color currents in response to a charge electric field, and the production of charge or color currents in response to a color electric field. This is reflected in the four types of conductances; however, we only need to identify three of them due to a generalized Onsager relation $\sigma_{yx}^{\rm coch} = -\sigma_{xy}^{\rm chco}$. In condensed-matter systems, typical Hall setups attempt to measure charge (ch) and spin (sp) currents in response to electric fields, such that only $\sigma_{yx}^{\rm chch}$ and $\sigma_{yx}^{\rm spch}$ are of interest [33,34]. However, in the context of cold atoms not only the response to fictitious charge electric fields but also the response to fictitious color electric fields may be accessible, thus allowing us to probe all four types of responses. In particular, it was noted recently that the color-color response is connected to a new type of topological invariant called the color-color Chern number [29,30]. To put this connection on solid ground, we discuss next the quantum Hall response for the Hamiltonian in Eq. (1) describing SU(3) fermions in two-dimensional optical lattices.

III. HALL CONDUCTANCES

In this section, we discuss the Hall response for SU(3) fermions using the Kubo formalism [35] and generalize a method developed to define proper spin currents when spin is not conserved in the context of SU(2) spin-1/2 systems [33,34] found in condensed matter.

Within the Kubo formalism, the generic Hall conductance is

$$\sigma_{yx}^{\lambda\tau} = \lim_{\delta\to 0} \frac{\hbar}{L_x L_y} \sum_{\{n\}\neq\{m\}} \chi(\{n\},\{m\}) \mathcal{F}_{yx}^{\lambda\tau}(\{n\},\{m\}), \tag{3}$$

where $(\{n\},\{m\})$ represent the sets of quantum numbers characterizing the eigenstates $|\{n\}\rangle$ of a given Hamiltonian with eigenvalues $E_{\{n\}}$. The first term, containing the Fermi functions $f_{\{n\}} = f(E_{\{n\}})$, is

$$\chi(\{n\},\{m\}) = \frac{f_{\{n\}} - f_{\{m\}}}{(E_{\{n\}} - E_{\{m\}})^2 + \delta^2} \tag{4}$$

and the current-current vertex function is

$$\mathcal{F}_{yx}^{\lambda\tau}(\{n\},\{m\}) = \mathrm{Im}\langle\{n\}|\hat{J}_y^\lambda|\{m\}\rangle\langle\{m\}|\hat{J}_x^\tau|\{n\}\rangle. \tag{5}$$

The operators in Eq. (5) are

$$\hat{J}_x^{\rm ch} = e\hat{v}_x I \tag{6}$$

for the charge current along x, where $\hat{v}_x = d\hat{x}/dt$, and I is the 3×3 identity matrix, while

$$\hat{J}_x^{\rm co} = \hbar\hat{v}_x J_\ell + \hbar\hat{x}\frac{dJ_\ell}{dt} \tag{7}$$

for the color current along x, where J_ℓ is the spin-1 matrix along the ℓ direction. Similar expressions apply along y. We note that the right-hand side in Eq. (7) contains the color-torque term dJ_ℓ/dt, which arises when color is not conserved. For SU(2) spin-1/2 fermions, this is analogous to the spin-torque term which must be present when spin is not conserved [33,34].

To study the Hall conductances associated with the Hamiltonian in Eq. (1), we need its eigenspectrum for rational flux ratios $\alpha = \Phi/\Phi_0 = p/q$, where p and q are relative prime integers, and Φ_0 is the quantum of flux. This eigenspectrum was recently investigated [36] for $\alpha = 1/3$. The filling factor ν is defined to be the average number of particles per site, therefore the maximum filling factor per site is 3, as there are at most three color states per site. Upon compactification of the xy plane into a torus, by imposing periodic boundary conditions along the x and y directions, one obtains $3q$ color bands within the magnetic Brillouin zone with momenta bounded by $-\pi/a_x \leqslant k_x \leqslant \pi/a_x$ and $-\pi/qa_y \leqslant k_y \leqslant \pi/qa_y$. The magnetic bands are then labeled by the band index n and momenta $\mathbf{k} = (k_x, k_y)$, and are obtained from $\hat{H}$ in its first quantization form [36]

$$\hat{H}(\hat{\mathbf{k}}) = \varepsilon_G(\hat{\mathbf{k}})I - h_x J_x - h_z(\hat{\mathbf{k}})J_z + b_z(\hat{\mathbf{k}})J_z^2, \tag{8}$$

where J_ℓ are spin-1 matrices, with $\ell = \{x, y, z\}$. The kinetic-energy operator for color c is

$$\varepsilon_c(\hat{\mathbf{k}}) = -2t_x\cos\left[(\hat{k}_x - k_{T_c})a_x\right] - 2t_y\cos[(\hat{k}_y - \mathcal{A}_y)a_y] \tag{9}$$

where $c = \{R, G, B\}$, and $k_{T_R} = +k_T$, $k_{T_G} = 0$, and $k_{T_B} = -k_T$. The color-flip field is h_x, the momentum-dependent Zeeman (color) field along the z axis is $h_z(\hat{\mathbf{k}}) = [\varepsilon_B(\hat{\mathbf{k}}) - \varepsilon_R(\hat{\mathbf{k}})]/2$, and the momentum-dependent quadratic Zeeman (color) field along the z axis is $b_z(\hat{\mathbf{k}}) = [\varepsilon_B(\hat{\mathbf{k}}) + \varepsilon_R(\hat{\mathbf{k}})]/2 - \varepsilon_G(\hat{\mathbf{k}})$. The term $b_z(\hat{\mathbf{k}})J_z^2$ describes the coupling of momentum and the color quadrupole tensor [37,38]. The presence of color fields h_x, $h_z(\hat{\mathbf{k}})$, and $b_z(\hat{\mathbf{k}})$ breaks SU(3) symmetry which is restored only when $h_x = 0$ for any value of k_T [30]. The terms representing color-orbit coupling $h_z(\hat{\mathbf{k}}) = 2t_x\sin(k_T a_x)\sin(\hat{k}_x a_x)$ and $b_z(\hat{\mathbf{k}}) = 4t_x\sin^2(k_T a_x/2)\cos(\hat{k}_x a_x)$ vanish when the color-orbit coupling parameter $k_T a_x = 0$. We remark that the $b_z(\hat{\mathbf{k}})J_z^2$ is absent for SU(2) spin-1/2 fermions in the presence of spin-orbit coupling. For SU(3) fermions, this term is responsible for the appearance of additional topological phases with nontrivial Chern numbers.

We note that a similar analysis can be done for higher irreducible representations (irreps) of SU(2), including the three-dimensional (spin-1) representation, as discussed in [30]. While the structure of the kinetic-energy operator for SU(2) spin-1 fermions is similar to that of SU(3) fermions, the corresponding interactions are very different. Furthermore, currently, SU(2) spin-1 fermions have not been experimentally realized and their interactions may exhibit density-density and spin-spin dependent terms. Thus, we focus our presentation on the SU(3) case and, in Sec. VIII B, we analyze the effects of SU(3)-symmetric interactions, which are realized in ^{173}Yb and ^{87}Sr, as discussed in the introduction. We emphasize that SU(3)-symmetric interactions are very important in considering the robustness of topological insulating phases with respect to this perturbation (see Sec. VIII B).

We highlight that the Hamiltonian in Eq. (8) is SU(3) symmetric only in the absence of external color-orbit and color-flip fields, that is, the kinetic-energy operator commutes with the Gell-Mann matrices [30]. This is also true for SU(3)-symmetric interactions, which are discussed in Sec. VIII B. However, we are interested in the quantum Hall response of SU(3) fermions when external color-orbit and color-flip fields are applied. Their presence introduces additional terms in the kinetic-energy operator, which no longer commutes with the Gell-Mann matrices, thus breaking SU(3) symmetry explicitly [30]. To understand the effects of external color fields on the quantum Hall response of SU(3) fermions, it is clear that one needs to break the SU(3) symmetry explicitly. This is no different from simpler cases such as the linear and nonlinear magnetic response of an initially SO(3) invariant ferromagnetic insulator, where the magnetic response can only be extracted in the presence of an external magnetic field, which breaks explicitly the original SO(3) symmetry.

For periodic boundary conditions (torus geometry) the Hall conductances associated with the Hamiltonian in Eq. (1) or Eq. (8) are given by the Kubo formula

$$\sigma_{yx}^{\lambda\tau} = \lim_{\substack{\delta\to 0\\ \mathbf{q}\to\mathbf{0}}} \frac{\hbar}{L_x L_y} \sum_{n\neq n',\mathbf{k}} \chi(n\mathbf{k}, n'\mathbf{k}+\mathbf{q}) \mathcal{F}_{yx}^{\lambda\tau}(n\mathbf{k}, n'\mathbf{k}+\mathbf{q}), \tag{10}$$

where the first term containing the Fermi functions $f_n(\mathbf{k}) = f[E_n(\mathbf{k})]$ is

$$\chi(n\mathbf{k}, n'\mathbf{k}+\mathbf{q}) = \frac{f_n(\mathbf{k}) - f_{n'}(\mathbf{k}+\mathbf{q})}{[E_n(\mathbf{k}) - E_{n'}(\mathbf{k}+\mathbf{q})]^2 + \delta^2} \tag{11}$$

and the current-current vertex function is

$$\mathcal{F}_{yx}^{\lambda\tau}(n\mathbf{k}, n'\mathbf{k}+\mathbf{q}) = \mathrm{Im}\langle n\mathbf{k}|\hat{J}_y^{\lambda}|n'\mathbf{k}+\mathbf{q}\rangle\langle n'\mathbf{k}+\mathbf{q}|\hat{J}_x^{\tau}|n\mathbf{k}\rangle. \tag{12}$$

The integrations in $\mathbf{k}$ are over the magnetic Brillouin zone, the energies $E_n(\mathbf{k})$ are the eigenvalues of $\hat{H}$ with $\alpha = p/q$, and $f_n(\mathbf{k})$ are the Fermi functions at $E_n(\mathbf{k})$. Notice that the states $|n\mathbf{k}\rangle$ are color spinor states with three components $\{R, G, B\}$ and that $\hat{J}_i^{\lambda}$ are operators representing both charge and color currents. The charge current operator is

$$\hat{J}_x^{\mathrm{ch}}(\mathbf{k}, \mathbf{k}+\mathbf{q}) = e\hat{v}_x(\mathbf{k}, \mathbf{k}+\mathbf{q})I \tag{13}$$

along x, where $\hat{v}_x(\mathbf{k}, \mathbf{k}+\mathbf{q}) = [\hat{v}_x(\mathbf{k}) + \hat{v}_x(\mathbf{k}+\mathbf{q})]/2$ is the symmetrized velocity operator $\hat{v}_x(\mathbf{k}) = (1/\hbar)\partial\hat{H}(\mathbf{k})/\partial k_x$ obtained from the Hamiltonian matrix $\hat{H}(\mathbf{k})$ in Eq. (8) describing the first quantization representation of the second-quantized Hamiltonian $\hat{H}$ in Eq. (1).

The color current operator is

$$\hat{J}_x^{\mathrm{co}}(\mathbf{k}, \mathbf{k}+\mathbf{q}) = \hbar\hat{v}_x(\mathbf{k}, \mathbf{k}+\mathbf{q})J_\ell + i\hbar\frac{\partial}{\partial q_x}\hat{\mathcal{T}}(\mathbf{k}, \mathbf{k}+\mathbf{q}) \tag{14}$$

along x, where $\hat{\mathcal{T}}(\mathbf{k}, \mathbf{k}+\mathbf{q}) = [\hat{\mathcal{T}}(\mathbf{k}) + \hat{\mathcal{T}}(\mathbf{k}+\mathbf{q})]/2$, with $\hat{\mathcal{T}}(\mathbf{k}) = dJ_\ell/dt = (1/i\hbar)[J_\ell, \hat{H}(\mathbf{k})]$ being the color torque that arises when color is not conserved. Similar expressions apply along the y direction.

The charge current contains only one term, and so does the corresponding charge-charge conductance. However, the color current contains two terms, one color conserving and the other with a color torque due to color nonconservation. This leads to color-charge and charge-color conductances with two contributions, and color-color conductance with four.

A general consequence of color nonconservation is that the color-charge, charge-color, and color-color Hall conductances are nonquantized. These Hall conductances are transport properties and thus involve the response of the system to external charge and color electric fields as shown in Eq. (2). Hall conductances are not ground-state properties as seen in Eq. (3), but they can be connected to a topological ground-state property when they are quantized. For spin-1/2 systems without spin-orbit coupling the quantization of the charge-charge Hall conductance was established first [21] and, not long after, it was realized that this quantization was associated with a topological invariant [39,40] characterized by the first Chern number of a U(1) principal fiber bundle on a torus [22]. This was a remarkable connection showing the direct proportionality of the charge-charge Hall conductance, which depends of the entire energy spectrum and eigenstates, to a Chern number that represents a topological quantity reflecting the ground-state wave function. To make deeper connections of this kind, we discuss next the Chern matrix for color SU(3) systems from which three different Chern numbers can be extracted: the charge-charge, the color-charge, and the color-color Chern numbers. To gain further insight into the nature of topological color insulators, it is imperative to establish the connection between the Hall conductances which are transport properties and the Chern numbers which are properties of the topological ground states.

IV. CHERN MATRIX AND CHERN NUMBERS

We apply general color-dependent phase twists ϕ_{xc} and $\phi_{yc'}$ to the ground-state wave function $|\Psi\rangle$ of the Hamiltonian in Eq. (1) or Eq. (8) with periodic boundary conditions (no edges), via the phase twist operator $U(\phi_{xc}, \phi_{yc'})$ leading to $|\widetilde{\Psi}\rangle = U(\phi_{xc}, \phi_{yc'})|\Psi\rangle$. This leads to a generalization of the SU(2) spin-1/2 Chern matrix [41,42] applicable to color SU(3) fermions in the fundamental representation [30]

$$\mathcal{C}_{cc'} = \frac{i}{4\pi}\iint d\phi_{xc} d\phi_{yc'} \mathcal{K}_{xy}(\phi_{xc}, \phi_{yc'}), \tag{15}$$

where the purely imaginary *curvature* function

$$\mathcal{K}_{xy}(\phi_{xc},\phi_{yc'}) = \left\langle \frac{\partial\widetilde{\Psi}}{\partial\phi_{xc}} \middle| \frac{\partial\widetilde{\Psi}}{\partial\phi_{yc'}} \right\rangle - \left\langle \frac{\partial\widetilde{\Psi}}{\partial\phi_{yc'}} \middle| \frac{\partial\widetilde{\Psi}}{\partial\phi_{xc}} \right\rangle, \quad (16)$$

where the integrations are over $0 \leqslant \phi_{xc} < 2\pi$ and $0 \leqslant \phi_{yc'} < 2\pi$. Here, we analyze only the fundamental representation of SU(3), in which case the Chern number matrix is 3×3, with $c = \{R, G, B\}$.

The matrix elements $\mathcal{C}_{cc'}$ of the Chern matrix $\mathcal{C}$ are integers provided that the chemical potential lies in a bulk band gap of the Hamiltonian in Eq. (1), a property that is a natural extension of SU(2) spin-1/2 systems [42]. From $\mathcal{C}$, we can define four scalar topological invariants by projecting into the charge $|\mathrm{ch}\rangle = (111)^T$ and color $|\mathrm{co}\rangle = (10\bar{1})^T$ vectors, where T means transposition and $\bar{1} = -1$. The first two scalar topological invariants are the charge-charge Chern number

$$C^{\mathrm{chch}} = \langle \mathrm{ch}|\mathcal{C}|\mathrm{ch}\rangle = \sum_{cc'} \mathcal{C}_{cc'} \quad (17)$$

and the color-charge Chern number

$$C^{\mathrm{coch}} = \langle \mathrm{co}|\mathcal{C}|\mathrm{ch}\rangle = \sum_{cc'} m_c \mathcal{C}_{cc'}. \quad (18)$$

The other two topological invariants are the charge-color Chern number

$$C^{\mathrm{chco}} = \langle \mathrm{ch}|\mathcal{C}|\mathrm{co}\rangle = \sum_{cc'} \mathcal{C}_{cc'} m_{c'} \quad (19)$$

and the color-color Chern number

$$C^{\mathrm{coco}} = \langle \mathrm{co}|\mathcal{C}|\mathrm{co}\rangle = \sum_{cc'} m_c \mathcal{C}_{cc'} m_{c'} \quad (20)$$

where m_c is the color quantum number with $m_R = +1$, $m_G = 0$, and $m_B = -1$. Since the Chern matrix is real and symmetric, the relation $C^{\mathrm{coch}} = C^{\mathrm{chco}}$ holds and there are only three independent scalar topological invariants: C^{chch}, C^{coch}, and C^{coco}. In general these invariants can have different values when the chemical potential lies within the same bulk gap. When color is conserved, $\mathcal{C}$ is diagonal and the Chern numbers simplify to $\mathcal{C}^{\mathrm{chch}} = \sum_c \mathcal{C}_{cc}$, $\mathcal{C}^{\mathrm{coch}} = \sum_c m_c \mathcal{C}_{cc}$, and $\mathcal{C}^{\mathrm{coco}} = \sum_c m_c^2 \mathcal{C}_{cc}$. It was recently pointed out [30] that $\mathcal{C}^{\mathrm{coco}}$ provides additional information about the ground state of topological color insulators since quite generally $\mathcal{C}^{\mathrm{coco}} \neq \mathcal{C}^{\mathrm{chch}}$ or $\mathcal{C}^{\mathrm{coch}}$. This should be contrasted to the SU(2) spin-1/2 case, where $\mathcal{C}^{\mathrm{spsp}} = \mathcal{C}^{\mathrm{chch}}$, and thus the spin-spin Chern number $\mathcal{C}^{\mathrm{spsp}}$ plays no additional role in the topological classification of topological insulators, which require only the charge-charge $\mathcal{C}^{\mathrm{chch}}$ and the spin-charge $\mathcal{C}^{\mathrm{spch}}$ Chern numbers [26,27].

V. CONNECTION BETWEEN CHERN NUMBERS AND HALL CONDUCTANCES

As we emphasized earlier the Hall conductances of SU(3) fermions are transport properties describing the charge and color current responses to external charge and color electric fields, thus they do not describe a property of the unperturbed ground state and are not necessarily quantized. In contrast the Chern numbers identified above are intrinsically a property of the ground-state wave function of the system, and provided that the chemical potential lies in a bulk gap, all the Chern numbers defined are integers. When charge and color are conserved, we can directly relate all Chern numbers to quantized Hall conductances. However, when color is not conserved the Hall conductances with a color component are not quantized and are not directly related to Chern numbers. Therefore, $\sigma_{yx}^{\mathrm{coch}}$, $\sigma_{yx}^{\mathrm{chch}}$, and $\sigma_{yx}^{\mathrm{coco}}$ are no longer useful for a direct extraction of the topological numbers $\mathcal{C}^{\mathrm{coch}}$, $\mathcal{C}^{\mathrm{chco}}$, and $\mathcal{C}^{\mathrm{coco}}$ that characterize the insulating ground states of the system.

Charge and color are strictly conserved when color-orbit coupling $k_T = 0$ and the color-flip field $h_x = 0$. However, when $k_T = 0$ and $h_x \neq 0$ the color projection state $|c_x\rangle \equiv |m_{c_x}\rangle$, which is an eigenstate of J_x, is also an eigenstate of the Hamiltonian matrix $\hat{H}(\hat{\mathbf{k}})$, therefore the color projection quantum number m_{c_x} along the x axis can be used to label the eigenstates of $\hat{H}(\hat{\mathbf{k}})$. At zero temperature, the charge-charge Hall conductance $\sigma_{yx}^{\mathrm{chch}}$ from Eq. (3) becomes

$$\sigma_{yx}^{\mathrm{chch}} = \frac{\hbar}{L_x L_y} \sum_{m\neq n,\mathbf{k}} \frac{\mathrm{Im}\langle u_{n\mathbf{k}}|\hat{\mathcal{J}}_y^{\mathrm{ch}}|u_{m\mathbf{k}}\rangle\langle u_{m\mathbf{k}}|\hat{\mathcal{J}}_x^{\mathrm{ch}}|u_{n\mathbf{k}}\rangle}{(E_{n\mathbf{k}} - E_{m\mathbf{k}})^2 + \delta^2}, \quad (21)$$

where the limit $\delta \to 0$ is taken at the end of the calculation. Here, n labels the ground state of the system with three-component wave function $|u_n(\mathbf{k})\rangle$ indexed by the color label c_x, while m labels the excited states with three-component wave function $|u_m(\mathbf{k})\rangle$ also indexed by the color label c_x. The charge current matrix operator is diagonal in color space $\hat{\mathcal{J}}_\ell^{\mathrm{ch}} = e\hat{v}_\ell I$ for each color component c_x, where $\hat{v}_\ell = (1/\hbar)\partial\hat{H}(\mathbf{k})/\partial k_\ell$ is the velocity operator along direction $\ell = \{x, y\}$ and I is the identity matrix for colors.

Using the phase twist transformation $U(\phi_{xc_x}, \phi_{yc'_x})$ for the ground-state wave function, and following the standard procedure to obtain Chern numbers from the Hall response [21,39,40], we arrive at the expected result

$$\sigma_{yx}^{\mathrm{chch}} = \frac{e^2}{h} \sum_{c_x c'_x} \mathcal{C}_{c_x c'_x} = \frac{e^2}{h} \mathcal{C}^{\mathrm{chch}}, \quad (22)$$

where $\mathcal{C}_{c_x c'_x}$ is the Chern matrix defined in Eq. (15), when the chemical potential lies within a bulk energy gap.

When the color operator J_x is conserved, the corresponding color-torque term $\hat{\mathcal{T}} = dJ_x/dt = 0$, and we write the color-current operator as $\hat{\mathcal{J}}_\ell^{\mathrm{co}} = \hbar\hat{v}_\ell J_x$, which is written in symmetrized form via the anticommutator $\hat{\mathcal{J}}_\ell^{\mathrm{co}} = \frac{\hbar}{2}\{\hat{v}_\ell, J_x\}$. At zero temperature, the color-charge Hall conductance $\sigma_{yx}^{\mathrm{coch}}$ reduces to

$$\sigma_{yx}^{\mathrm{coch}} = \frac{\hbar}{L_x L_y} \sum_{m\neq n,\mathbf{k}} \frac{\mathrm{Im}\langle u_{n\mathbf{k}}|\hat{\mathcal{J}}_y^{\mathrm{co}}|u_{m\mathbf{k}}\rangle\langle u_{m\mathbf{k}}|\hat{\mathcal{J}}_x^{\mathrm{ch}}|u_{n\mathbf{k}}\rangle}{(E_{n\mathbf{k}} - E_{m\mathbf{k}})^2 + \delta^2}. \quad (23)$$

Using the same phase twist transformations for the wave functions discussed previously, we arrive at the result

$$\sigma_{yx}^{\mathrm{coch}} = \frac{e}{2\pi} \sum_{c_x c'_x} m_{c_x} \mathcal{C}_{c_x c'_x} = \frac{e}{2\pi} \mathcal{C}^{\mathrm{coch}}, \quad (24)$$

where $\mathcal{C}_{c_x c'_x}$ is the Chern matrix and the result is valid as long as the chemical potential lies inside of a bulk gap. An analogous expression is obtained for the charge-color Hall

conductance $\sigma_{yx}^{\mathrm{chco}}$ leading to

$$\sigma_{yx}^{\mathrm{chco}} = \frac{e}{2\pi}\sum_{c_x c_x'} \mathcal{C}_{c_x c_x'} m_{c_x'} = \frac{e}{2\pi}\mathcal{C}^{\mathrm{chco}}. \tag{25}$$

At zero temperature, the color-color Hall conductance $\sigma_{yx}^{\mathrm{coco}}$ has only one contribution when color is conserved, since the color torque vanishes, $\hat{\mathcal{T}} = 0$, leading to

$$\sigma_{yx}^{\mathrm{coco}} = \frac{\hbar}{L_x L_y}\sum_{m\neq n,\mathbf{k}} \frac{\mathrm{Im}\langle u_{n\mathbf{k}}|\hat{\mathcal{J}}_y^{\mathrm{co}}|u_{m\mathbf{k}}\rangle\langle u_{m\mathbf{k}}|\hat{\mathcal{J}}_x^{\mathrm{co}}|u_{n\mathbf{k}}\rangle}{(E_{n\mathbf{k}} - E_{m\mathbf{k}})^2 + \delta^2}. \tag{26}$$

From this expression, we obtain

$$\sigma_{yx}^{\mathrm{coco}} = \frac{\hbar}{2\pi}\sum_{c_x c_x'} m_{c_x} C_{c_x c_x'} m_{c_x'} = \frac{\hbar}{2\pi}C^{\mathrm{coco}}, \tag{27}$$

which is valid as long as the chemical potential lies inside of a bulk gap.

Notice that $\sigma_{yx}^{\mathrm{chch}}$ is expressed in units of e^2/h, $\sigma_{yx}^{\mathrm{coch}}$ and $\sigma_{yx}^{\mathrm{chco}}$ are expressed in units of $e/2\pi$, and $\sigma_{yx}^{\mathrm{coco}}$ is expressed in units of $\hbar/2\pi$, while the corresponding SU(2) spin-1/2 units are e^2/h for $\sigma_{yx}^{\mathrm{chch}}$, $e/4\pi$ for $\sigma_{yx}^{\mathrm{spch}}$ and $\sigma_{yx}^{\mathrm{chsp}}$, and $\hbar/4\pi$ for $\sigma_{yx}^{\mathrm{spsp}}$.

When J_x is not conserved, that is, when the color-orbit coupling $k_T \neq 0$, the Hall conductances $\sigma_{yx}^{\mathrm{coch}}$, $\sigma_{yx}^{\mathrm{chco}}$, and $\sigma_{yx}^{\mathrm{coco}}$ are no longer proportional to Chern numbers, and thus these color Hall conductances are no longer quantized. Nevertheless, when the chemical potential lies inside of the bulk gap, the Chern numbers obtained from the Chern matrix define a set of topological invariants that characterize the insulating ground state. In other words, the color-related Chern numbers do not depend explicitly on the conservation of J_x as they are traced over all color labels, while the Hall conductances explicitly depend on the color torque $\hat{\mathcal{T}}$ when J_x is not conserved. When $k_T \neq 0$, the calculation of color-Hall conductances requires the inclusion of color-torque terms involving dJ_x/dt in the color-current operator $\hat{\mathcal{J}}_\ell^{\mathrm{co}} = d(\hat{\mathbf{r}}_\ell \hbar J_x)/dt$.

We show in Fig. 2 plots of Chern numbers and corresponding Hall conductances versus chemical potential μ/t_y, which are compatible to parameters $\alpha = 1/3, t_x/t_y = 1, k_T a_x = \pi/8$, and $h_x/t_y = 2$. Although color nonconserving contributions affect transport properties like the color-Hall conductances and generally cause deviations from their exact quantization, the Chern matrix and its associated Chern numbers, which are ground-state properties obtained through phase twists, remain integers and can be used to distinguish topological color insulators from conventional color insulators, even in cases where the color-Hall conductances are not quantized. In other words, the Chern numbers are a more fundamental property of topological insulators, and the nonquantization of Hall conductances with a color component is not sufficient to rule out if a phase is topological or not. This has a direct parallel to quantum spin-Hall phases, where even when the spin-Hall conductance is not quantized, a Z_2 topological invariant can be used to distinguish a topological spin-Hall phase with quantized or nonquantized spin-Hall conductance from a conventional insulator [26]. Our findings are also consistent with the usage of the charge-charge and spin-charge Chern numbers as topological invariants characterizing *weak*

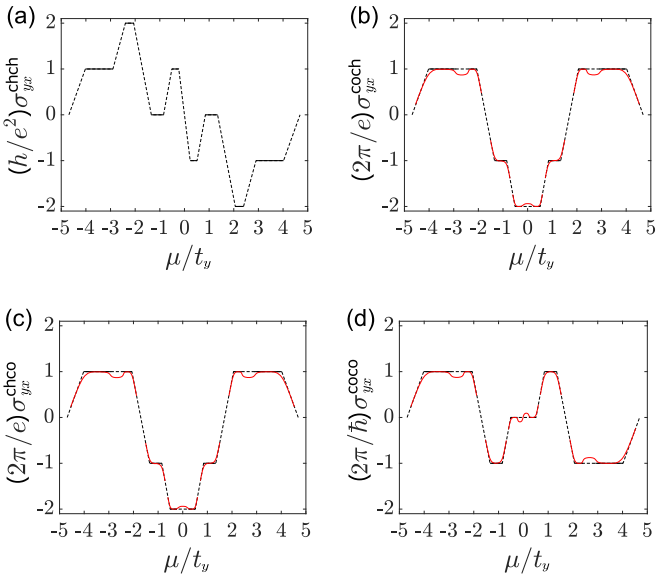

FIG. 2. Hall conductances $\sigma_{yx}^{\lambda\tau}$ and Chern numbers $\mathcal{C}^{\lambda\tau}$, with $\lambda, \tau = \{\mathrm{ch}, \mathrm{co}\}$, vs chemical potential μ/t_y. The parameters used are $\alpha = 1/3$, $t_x/t_y = 1$, $h_x/t_y = 2$, and $k_T a_x = \pi/8$, corresponding to a color nonconserving case. The Chern numbers in the bulk gaps are shown as the solid black plateaus, and the corresponding Hall conductances are shown as solid red lines. The dashed black lines are guides to the eye. In (a) $\sigma_{yx}^{\mathrm{chch}} = (e^2/h)\mathcal{C}^{\mathrm{chch}}$ inside bulk gaps, because charge is conserved; however, in (b), (c), and (d) the other Hall conductances $\sigma_{yx}^{\mathrm{coch}}$, $\sigma_{yx}^{\mathrm{chco}}$, and $\sigma_{yx}^{\mathrm{coco}}$ are not quantized within the bulk gaps, and thus are not proportional to the Chern numbers $\mathcal{C}^{\mathrm{coch}}$, $\mathcal{C}^{\mathrm{chco}}$, and $\mathcal{C}^{\mathrm{coco}}$, due to the presence of color torques. The contributions of color torques are small for these parameters, but already show the absence of quantization of the Hall conductances with a color component.

topological spin-Hall phases in honeycomb (graphenelike) lattices for spin-1/2 fermions [27,28], where time-reversal symmetry is broken, and the spin-Hall conductance is not quantized.

Before concluding this section, we would like to mention that the generalization for SU(N) fermions in the fundamental representation, with $N > 3$ flavors, is trivial, in which case the Chern matrix becomes $N \times N$. The Chern numbers are defined similarly, that is, we have a charge-charge Chern number C^{chch}, a charge-flavor Chern number C^{chfl}, a flavor-charge Chern number C^{flch}, and a flavor-flavor Chern number C^{flfl}. Just like in the SU(3) case, the flavor-flavor Chern number provides additional topological information about the SU(N) insulating states. For higher irreducible representations of SU(3) or SU(N), additional Chern numbers emerge, and the topological classification of flavor insulators becomes more complex as mentioned in our earlier work [30], however we postpone this rather elaborate analysis for a future investigation.

VI. BULK-EDGE CORRESPONDENCE FOR SU(3) FERMIONS

For the conventional quantum Hall effect, the bulk Hall conductance on a torus (obtained by imposing periodic bound-

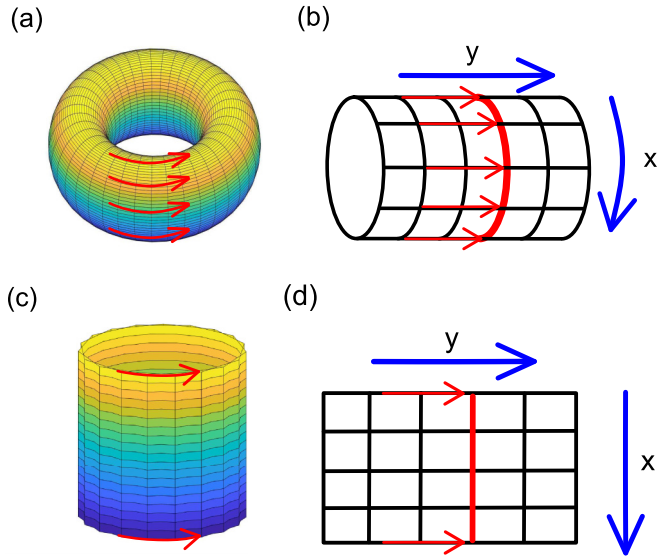

FIG. 3. Schematics showing the toroidal and cylindrical geometries. (a) The torus geometry with periodic boundary conditions along x and y. (b) The Hall currents along y over a section of the torus. (c) The cylinder geometry with finite size along x and periodic boundary conditions along y. (d) The Hall current along y over a section of the cylinder.

ary conditions in the xy plane) and the Hall conductance associated with edge states are identical [23,24]. This is the bulk-edge correspondence for the Hall conductances. Because the number of particles is conserved, Hall conductances in bulk gaps are quantized and directly proportional to Chern numbers, which reflect the number of chiral edge states within the bulk gap. The bulk-edge correspondence allows experimentalists to access Chern numbers characterizing the ground-state wave function (on a torus) of a system with chemical potential within a bulk gap, that is, one can make an edge measurement to extract a bulk topological property.

For SU(3) fermions, we also show that a bulk-edge correspondence exists between the bulk Hall conductances and those associated with edge states, which physically implies that a measurement of the Hall responses in a sample without edges (toroidal geometry) and one in a sample with edges (realistic geometry) ideally yield the same results (see Fig. 3). This means, that we can rely on measurements of samples with edges to extract the Hall conductances on a torus. When color is conserved, the bulk-edge correspondence implies that edge measurements should reveal the quantization of bulk color-related Hall conductances and allow for the extraction of Chern numbers $\mathcal{C}^{\rm coch}$, $\mathcal{C}^{\rm chco}$, and $\mathcal{C}^{\rm coco}$. However, when color is not conserved, the color-related Hall conductances are no longer quantized for chemical potentials lying inside a bulk gap, so their measurement on samples with edges no longer provides direct access to the desired Chern numbers.

Consider the local three-component color field operator $\mathbf{\Phi}(\mathbf{r}) = [\phi_R(\mathbf{r}), \phi_G(\mathbf{r}), \phi_B(\mathbf{r})]^T$. The charge density $e\hat{\rho}(\mathbf{r}) = e\mathbf{\Phi}^\dagger(\mathbf{r})\mathbf{\Phi}(\mathbf{r})$ satisfies its continuity equation

$$e\partial\hat{\rho}(\mathbf{r})/\partial t + \nabla\cdot\hat{\mathbf{J}}^{\rm ch}(\mathbf{r}) = 0, \tag{28}$$

where $\hat{\mathbf{J}}^{\rm ch}(\mathbf{r}) = {\rm Re}\mathbf{\Phi}^\dagger(\mathbf{r})e\hat{\mathbf{v}}\mathbf{\Phi}(\mathbf{r})$, with $\hat{\mathbf{v}} = d\hat{\mathbf{r}}/dt$ being the velocity operator. The color magnetization density $\hbar\hat{J}_\ell(\mathbf{r}) = \hbar\mathbf{\Phi}^\dagger(\mathbf{r})J_\ell\mathbf{\Phi}(\mathbf{r})$ satisfies its continuity equation

$$\hbar\partial\hat{J}_\ell(\mathbf{r})/\partial t + \nabla\cdot\hat{\mathbf{J}}^{\rm co}(\mathbf{r}) = 0, \tag{29}$$

where $\hat{\mathbf{J}}^{\rm co}(\mathbf{r}) = {\rm Re}\mathbf{\Phi}^\dagger(\mathbf{r})d(\hat{\mathbf{r}}\hbar J_\ell)/dt\mathbf{\Phi}(\mathbf{r})$, These expressions are generalizations of the SU(2) spin-1/2 case [34], and are manifestations of the conserved Noether currents. Because of these conservation laws, a change in boundary conditions along x can only affect the local current distributions (like currents flowing in the bulk or at the edges), but cannot affect the flux of the current densities flowing along the y direction. As a result, the total currents flowing along y in the torus or edge geometries must be the same, that is, $(\mathcal{J}_y^\lambda)_{\rm torus} = (\mathcal{J}_y^\lambda)_{\rm edges}$ with $\lambda = \{{\rm ch}, {\rm co}\}$. Therefore, from Eq. (2), the Hall conductances $(\sigma_{yx}^{\lambda\tau})_{\rm torus} = (\sigma_{yx}^{\lambda\tau})_{\rm edges}$. This general result is the bulk-edge correspondence for the Hall conductances.

For a finite system along the x direction and periodic boundary conditions along y, a direct calculation of the Hall conductivities can be performed using the generic Kubo formula from Eq. (3). In this case, it is convenient to work in a mixed representation, that is, in real space along x and in momentum space along y. The mapping of the states is $|\{n\}\rangle \to |n, k_y\rangle$, $|\{m\}\rangle \to |n', k_y + q_y\rangle$, while for the Hamiltonian it is $\hat{H} \to \hat{H}(x, k_y)$. Along x, we use the current operators in their real space representation $J_x^{\rm ch} = ed\hat{x}/dtI$ and $J_x^{\rm co} = \hbar(d\hat{x}/dt)J_\ell + \hbar\hat{x}dJ_\ell/dt$, with $d\hat{x}/dt = (1/i\hbar)[\hat{x}, \hat{H}(x, k_y)]$. Along y, we use the current operator in the momentum space representation $J_y^{\rm ch} = e\hat{v}_yI$ and $J_y^{\rm co} = \hbar\hat{v}_yJ_\ell + i\hbar\partial/\partial q_ydJ_\ell/dt$, with $dJ_\ell/dt = (1/i\hbar)[J_\ell, \hat{H}(x, k_y)]$. Direct computations of the Hall conductances lead again to the bulk-edge correspondence stated above.

Having established the bulk-edge correspondence for the Hall conductances, and the conditions under which the Hall conductances relate to the Chern numbers obtained from the Chern matrix, we turn our attention to some properties of the edge states.

VII. EDGE STATES AND COLOR MAGNETIZATION

We analyze a few examples of edge states and their magnetizations. To be specific, we discuss regions of the energy spectrum near particular values of the chemical potential μ corresponding to flux ratio $\alpha = 1/3$, hoppings $t_x/t_y = 1$, color-flip field $h_x/t_y = 2$, and color-orbit couplings $k_Ta_x = 0$ or $\pi/8$, and analyze the wave function and magnetization of the corresponding edge states.

The local color magnetization density can be written in terms of the eigenfunctions of the Hamiltonian $\hat{H}$ in Eq. (1) or Eq. (8) as

$$\mathcal{M}_\ell(x, y) = \hbar\mathbf{\Phi}^\dagger(x, y)J_\ell\mathbf{\Phi}(x, y), \tag{30}$$

where $\mathbf{\Phi}(x, y)$ is a color spinor with three components and J_ℓ are the spin-1 matrices with $\ell = \{x, y, z\}$. Since the coordinates x and y are uncoupled, the eigenfunctions can be written as the product $\boldsymbol{\phi}(x)\varphi(y)$, where $\boldsymbol{\phi}(x)$ is a color spinor with three components $[\phi_R(x), \phi_G(x), \phi_B(x)]^T$ or $[\phi_\uparrow(x), \phi_0(x), \phi_\downarrow(x)]^T$, where the symbol T indicates transposition, and $\varphi(y)$ is a scalar wave function along y. To explore

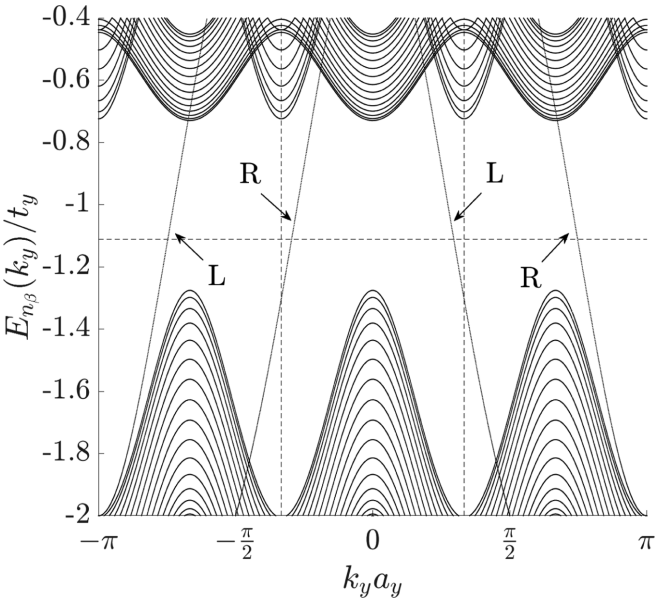

FIG. 4. Eigenvalues $E_{n_\beta}(k_y)$ vs $k_y a_y$ for magnetic flux ratio $\alpha = 1/3$, $t_x/t_y = 1$, $k_T a_x = 0$, and $h_x/t_y = 2$. The bulk bands have periodicity $2\pi/3a_y$, and the edge bands have periodicity $2\pi/a_y$ along the k_y direction. The dashed horizontal line indicates the chemical potential $\mu/t_y = -1.07$ and the labels R (right) and L (left) characterize the location of the edge states. The Chern numbers in this phase are $\mathcal{C}^{\text{chch}} = 0$, $\mathcal{C}^{\text{coch}} = -1$, and $\mathcal{C}^{\text{coco}} = -1$, while the filling factor is $\nu = 1$.

edge states, we consider a system with $N_s = 50$ sites along the x direction with open boundary conditions, but periodic along y, where momentum k_y is conserved.

To keep the presentation simple, we discuss only the color magnetization

$$M_\ell(x) = \sum_y \mathcal{M}(x, y) = \hbar \boldsymbol{\phi}^\dagger(x) J_\ell \boldsymbol{\phi}(x) \tag{31}$$

for all three spatial directions $\ell = \{x, y, z\}$.

In Fig. 4, we plot the energy dispersion $E_{n_\beta}(k_y)$ for flux ratio $\alpha = 1/3$, $t_x/t_y = 1$, $h_x/t_y = 2$, $k_T a_x = 0$, and chemical potential $\mu/t_y = -1.07$. The Chern numbers in this phase are $\mathcal{C}^{\text{chch}} = 0$, $\mathcal{C}^{\text{coch}} = -1$, and $\mathcal{C}^{\text{coco}} = -1$, while the filling factor is $\nu = 1$. Notice that the identification of edge states alternates between right (R) and left (L) edges with increasing k_y. Since there are two pairs of edge states inside the bulk gap with opposite chirality, the total chirality is zero and charge-charge Chern number vanishes. Since the color-orbit parameter is $k_T a_x = 0$, the color projection along the x axis is conserved, that is, the commutator $[J_x, \hat{H}(\mathbf{k})] = 0$, where $\hat{H}(\mathbf{k})$ is the Hamiltonian matrix in momentum space from Eq. (8). This means that the eigenstates $|c_x\rangle$ of J_x are also eigenstates of $\hat{H}(\mathbf{k})$ with color quantum numbers m_{c_x}.

In Fig. 5, we plot the color magnetization components $M_\ell(x)$ in Fig. 5(a), as well as the modulus of $|\phi_c(x)|$ of each wave-function component $\phi_c(x)$, where $c = \{R, G, B\}$ or $\{\uparrow, 0, \downarrow\}$. The left ($L$) edge state represented in Fig. 5(a) is a mixed color state, but is the eigenstate $|\uparrow_x\rangle$ of J_x, as can be seen also from the color magnetization components $M_\ell(x)$. In this case the *integrated* magnetization $\widetilde{M}_x = \sum_x M_x(x)$ is

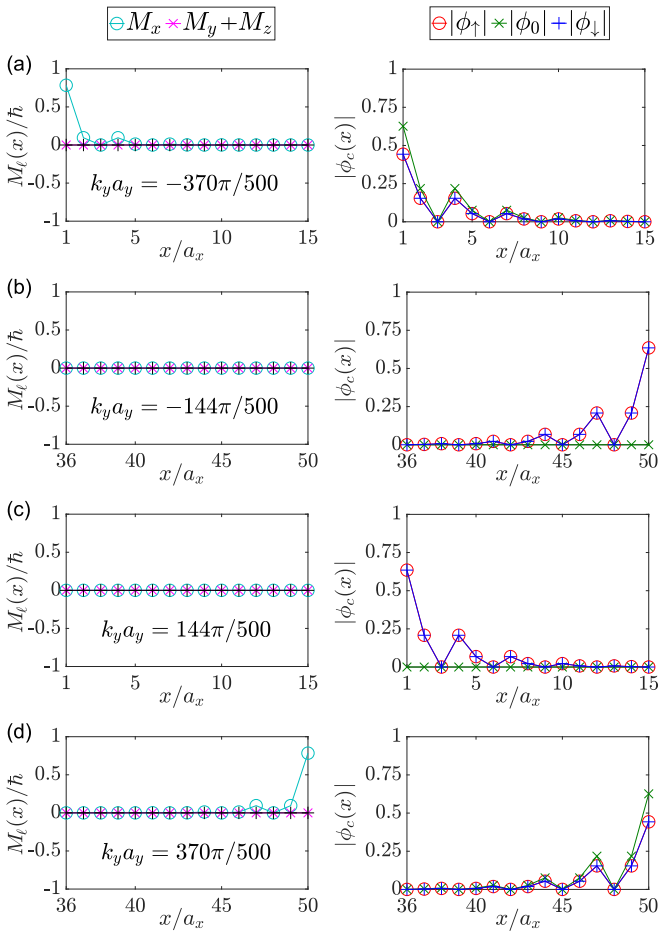

FIG. 5. In each panel (a)–(d), the color magnetizations $M_\ell(x)$ (in units of $\hbar$) for $\ell = \{x, y, z\}$ are shown in the left panels and the moduli of the color spinor components $|\phi_c(x)|$, where $c = \{R, G, B\}$ or $\{\uparrow, 0, \downarrow\}$, are shown in the right panels. The parameters used are the same as in Fig. 4, that is, $\alpha = 1/3$, $t_x/t_y = 1$, $h_x/t_y = 2$, $k_T a_x = 0$, and $\mu/t_y = -1.07$. The order in which the edge states appear is identical to that seen in Fig. 4, as indicated in each panel by the value of the momentum k_y.

exactly equal to $+1$ (in units of $\hbar$), while the *integrated* magnetizations $\widetilde{M}_y = \sum_x M_y(x)$ and $\widetilde{M}_z = \sum_x M_z(x)$ are exactly equal to zero. The right (R) edge state represented in Fig. 5(b) is a mixed color state, but is the eigenstate $|0_x\rangle$ of J_x, as can also be inferred from the color magnetization components $M_\ell(x)$, as it corresponds to a zero color magnetization state. Therefore, all *integrated* magnetizations vanish, that is, $\widetilde{M}_x = \widetilde{M}_y = \widetilde{M}_z = 0$.

Similarly, the left (L) edge state represented in Fig. 5(c) is a mixed color state, but is the eigenstate $|0_x\rangle$ of J_x, leading to a zero magnetization state with $\widetilde{M}_x = \widetilde{M}_y = \widetilde{M}_z = 0$, as in Fig. 5(b). Lastly, the right (R) edge state represented in Fig. 5(d) is a mixed color state, but is the eigenstate $|\uparrow_x\rangle$ of J_x, leading to *integrated* magnetizations $\widetilde{M}_x = +1$ (in units of $\hbar$), $\widetilde{M}_y = \widetilde{M}_z = 0$, as in Fig. 5(a). The states shown in Figs. 5(b) and 5(c) are chiral pairs with chirality $+1$ and color projection $m_{c_x} = 0$, while the states shown in Figs. 5(a) and 5(d) are chiral pairs with chirality -1 and color projection $m_{c_x} = +1$.

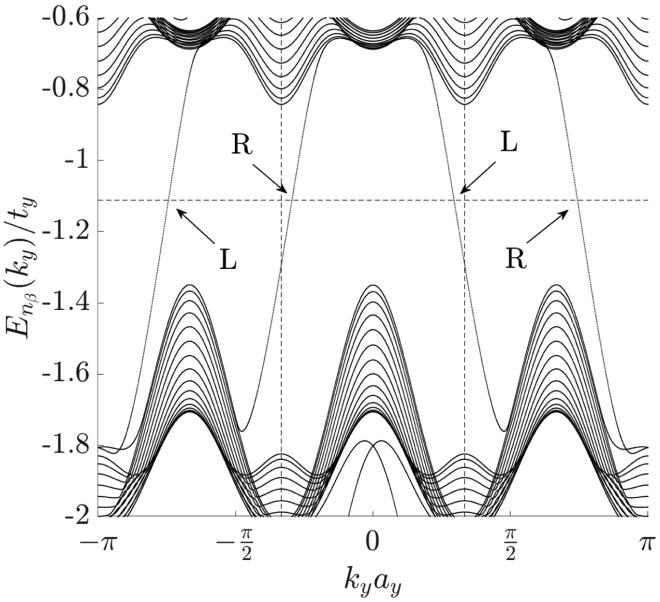

FIG. 6. Eigenvalues $E_{n_\beta}(k_y)$ vs $k_y a_y$ for magnetic flux ratio $\alpha = 1/3$, $t_x/t_y = 1$, $k_T a_x = \pi/8$, and $h_x/t_y = 2$. The bulk bands have periodicity $2\pi/3a_y$, and the edge bands have periodicity $2\pi/a_y$ along the k_y direction. The dashed horizontal line indicates the chemical potential $\mu/t_y = -1.11$ and the labels R (right) and L (left) characterize the location of the edge states. The Chern numbers in this phase are $\mathcal{C}^{\text{chch}} = 0$, $\mathcal{C}^{\text{coch}} = -1$, and $\mathcal{C}^{\text{coco}} = -1$, while the filling factor is $\nu = 1$.

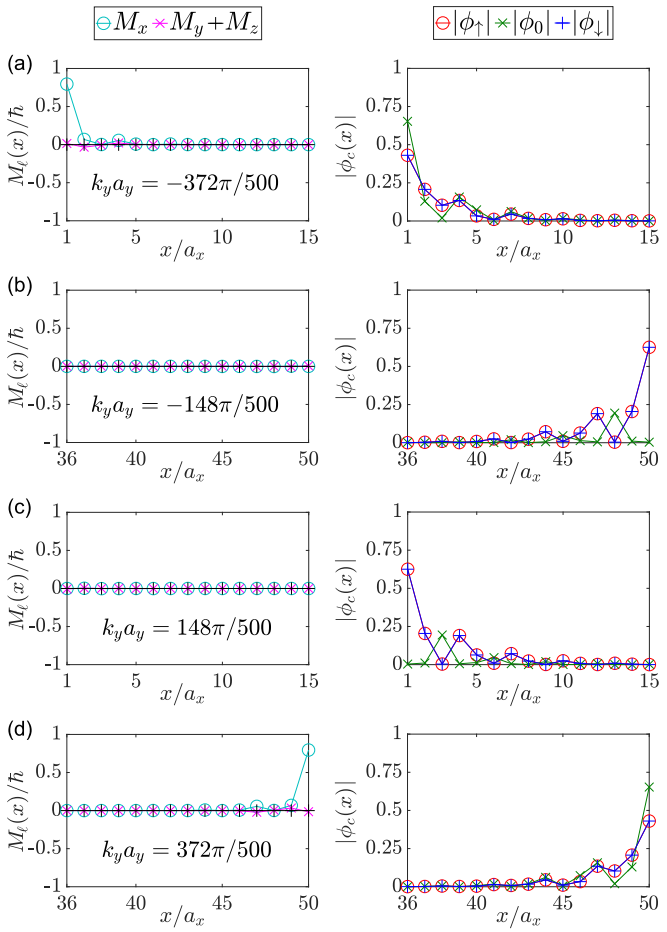

FIG. 7. In each panel (a)–(d), the color magnetizations $M_\ell(x)$ for $\ell = \{x, y, z\}$ are shown in the left panels and the moduli of the color spinor components $|\phi_c(x)|$, where $c = \{R, G, B\}$ or $\{\uparrow, 0, \downarrow\}$, are shown in the right panels. The parameters used are the same as in Fig. 6, that is, $\alpha = 1/3$, $t_x/t_y = 1$, $h_x/t_y = 2$, $k_T a_x = \pi/8$, and $\mu/t_y = -1.11$. The order in which the edge states appear is identical to that seen in Fig. 6, as indicated in each panel by the value of the momentum k_y.

In Fig. 6, we plot the energy dispersion $E_{n_\beta}(k_y)$ for $\alpha = 1/3$, $t_x/t_y = 1$, $h_x/t_y = 2$, $k_T a_x = \pi/8$, and chemical potential $\mu/t_y = -1.11$. The Chern numbers in this phase are $\mathcal{C}^{\text{chch}} = 0$, $\mathcal{C}^{\text{coch}} = -1$, and $\mathcal{C}^{\text{coco}} = -1$. In the bulk gap, there are two pairs of edge states with opposite chirality leading to the vanishing of charge-charge Chern number, that is, $C^{\text{chch}} = 0$. In Fig. 6, we highlight that the location of the edge states alternates between right (R) and left (L) edges with increasing k_y.

For $k_T a_x \neq 0$, the color operator J_x is no longer conserved since the color-orbit coupling causes a rotation $e^{ik_T x J_z}$ (color-gauge transformation) that mixes locally the color states $|\uparrow_x\rangle$, $|0_x\rangle$, $|\downarrow_x\rangle$. Given that the local color rotation is about the z axis, then a local color magnetization appears also along the y axis, but does not appear along z. For $k_T a_x = \pi/8$ the effect is small, but it can still be seen in the panels of Fig. 7. It is important to emphasize that the local color rotation is nonchiral, in the sense that it does not affect the chirality of the edge states. Furthermore, for states on the same edge the mixed color states are orthogonal. Lastly, for pairs of chiral edge states, the local magnetization $\mathcal{M}_x(x)$ is exactly the same on both edges, while the local magnetization $\mathcal{M}_y(x)$ has opposite signs for right (R) and left (L) edges.

The effects of $k_T a_x \neq 0$ on topological insulator states, which already exist when $k_T a_x = 0$, are not too dramatic from the magnetization perspective. Except for mixing the color states described above, the chirality of pairs of edge states is preserved, since the color-orbit coupling is nonchiral. The effects of $k_T a_x \neq 0$ are stronger in the regions where the energy bands overlap when $k_T a_x = 0$, in which case the color-orbit coupling lifts degeneracies of the bands and introduces new bulk gaps.

In Fig. 8, we plot the energy dispersion $E_{n_\beta}(k_y)$ for $\alpha = 1/3$, $t_x/t_y = 1$, $h_x/t_y = 2$, $k_T a_x = \pi/8$, and $\mu/t_y = -0.37$. The Chern numbers in this phase are $\mathcal{C}^{\text{chch}} = +1$, $\mathcal{C}^{\text{coch}} = -2$, and $\mathcal{C}^{\text{coco}} = 0$, while the filling factor is $\nu = 4/3$. At the chemical potential indicated by the dashed line, there are three pairs of chiral edge states; two of them have chirality $+1$ and the third has chirality -1 leading to a charge-charge Chern number $C^{\text{chch}} = +1$. We highlight the location of the edge states for chemical potential $\mu/t_y = -0.37$, and notice that the identification of edge states alternates between left (L) and right (R) edges with increasing k_y.

In Fig. 9, we plot the color magnetizations $M_\ell(x)$ for $\ell = \{x, y, z\}$ and the modulus of each color spinor component $|\phi_c(x)|$, where $c = \{R, G, B\}$ or $\{\uparrow, 0, \downarrow\}$. The parameters used are the same as in Fig. 8, that is, $\alpha = 1/3$, $t_x/t_y = 1$, $h_x/t_y = 2$, $k_T a_x = \pi/8$, and $\mu/t_y = -0.37$. Three pairs of edge states are shown. The states in panels (a) and (f) are chiral edge

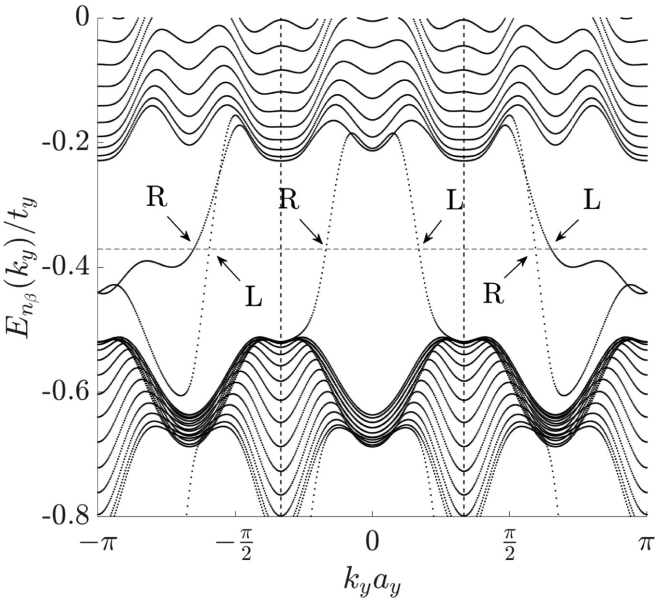

FIG. 8. Eigenvalues $E_{n_\beta}(k_y)$ vs $k_y a_y$ for magnetic flux ratio $\alpha = 1/3$, $t_x/t_y = 1$, $k_T a_x = \pi/8$, and $h_x/t_y = 2$. The bulk bands have periodicity $2\pi/3a_y$, and the edge bands have periodicity $2\pi/a_y$ along the k_y direction. The dashed horizontal line indicates the chemical potential $\mu/t_y = -0.37$ and the labels R (right) and L (left) characterize the location of the edge states. The Chern numbers in this phase are $\mathcal{C}^{\text{chch}} = +1$, $\mathcal{C}^{\text{coch}} = -2$, and $\mathcal{C}^{\text{coco}} = 0$, while the filling factor is $\nu = 4/3$.

pairs with chirality $+1$, *integrated* color magnetization $\widetilde{M}_x = \sum_x M_x(x)$ close to -1 (in units of $\hbar$) on both edges, a small positive *integrated* color magnetization $\widetilde{M}_y = \sum_x M_y(x)$ for the state on the right edge (a), and a small negative $\widetilde{M}_y$ for the state on the left edge (f). The states in panels (b) and (e) are chiral edge pairs with chirality -1, $\widetilde{M}_x$ close to -1 (in units of $\hbar$) on both edges, a small positive $\widetilde{M}_y$ for the state on the left edge (b), and a small negative $\widetilde{M}_y$ for the state on the right edge (e). The states in panels (c) and (d) are chiral edge pairs with chirality $+1$, $\widetilde{M}_x$ close to zero on both edges, a small positive $\widetilde{M}_y$ for the state on the right edge (c), and a small negative $\widetilde{M}_y$ for the state on the left edge (d). Notice that for pairs of chiral edge states, the local magnetization $\mathcal{M}_x(x)$ is exactly the same on both edges, while the local magnetization $\mathcal{M}_y(x)$ has opposite signs for right (R) and left (L) edges.

Having discussed edge states and their magnetizations for a few examples of topological insulating phases, we explore next the robustness of edge states to disorder and SU(3)-symmetric interactions. We link the existence of this robustness or its absence to Hall conductances and Chern numbers.

VIII. ROBUSTNESS OF EDGE STATES AGAINST DISORDER AND INTERACTIONS

In this section, we analyze the robustness of edge states with respect to disorder and SU(3)-symmetric interactions, which were preliminarily discussed in an earlier publication [30]. Our discussion not only addresses the idea of *strong* versus *weak* topological color insulators in analogy to

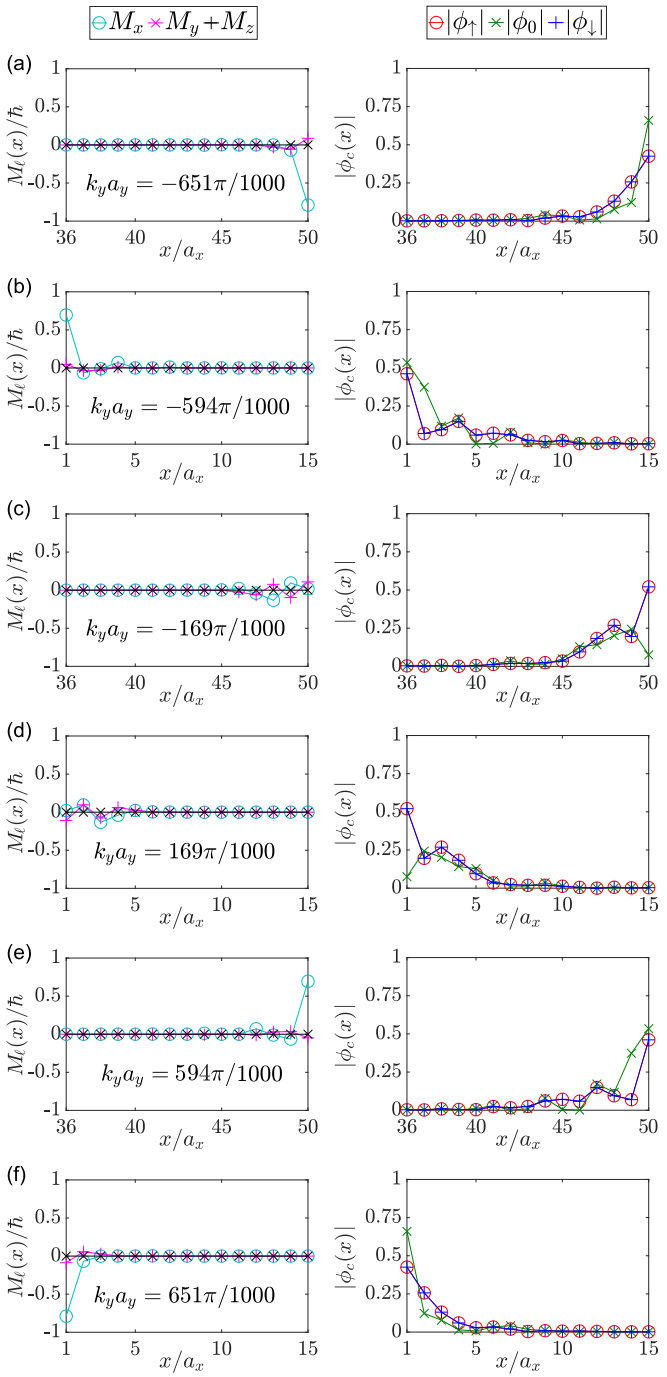

FIG. 9. In each panel (a)–(f), the magnetizations $M_\ell(x)$ for $\ell = \{x, y, z\}$ are shown in the left panels and the moduli of the color spinor components $|\phi_c(x)|$, where $c = \{R, G, B\}$ or $\{\uparrow, 0, \downarrow\}$, are shown in the right panels. The parameters used are the same as in Fig. 6, that is, $\alpha = 1/3$, $t_x/t_y = 1$, $h_x/t_y = 2$, $k_T a_x = \pi/8$, and $\mu/t_y = -0.37$. The order in which the edge states appear is identical to that seen in Fig. 8, as indicated in each panel by the value of the momentum k_y.

SU(2) spin-1/2 systems for graphenelike honeycomb lattices [27,28], but also introduces the concept of *intermediate* topological color insulators. We define *strong* topological color insulators as systems where either weak disorder or weak SU(3)-symmetric interactions do not affect the ability of all edge states to conduct. We define *intermediate* topological

color insulators as systems where either weak disorder or weak SU(3)-symmetric interactions affect the ability of some, but not all, edge states to conduct. We define *weak* topological color insulators as systems where either weak disorder or weak SU(3)-symmetric interactions affect the ability of all edge states to conduct.

To illustrate examples of this classification refinement, we discuss the robustness of edge states in three cases. The first two examples correspond to edge states shown in Figs. 4 and 6, where the bulk Chern numbers are $\mathcal{C}^{\rm chch}=0$, $\mathcal{C}^{\rm coch}=-1$, and $\mathcal{C}^{\rm coco}=-1$, while the filling factor is $\nu=1$. The last example corresponds to edge states shown in Fig. 8, where the bulk Chern numbers are $\mathcal{C}^{\rm chch}=+1$, $\mathcal{C}^{\rm coch}=-2$, and $\mathcal{C}^{\rm coco}=0$, while the filling factor is $\nu=4/3$.

A. Robustness of edge states against disorder

We emphasize that in cold atom systems, disorder is generally nonexistent unless created externally, that is, disorder is not an intrinsic property of optical lattices, but rather an extrinsic property that can be introduced by external speckle patterns [43,44], bichromatic disorder [45], or designed impurity potentials [46].

To understand the effects of weak local disorder, we review briefly a few symmetry properties of our Hamiltonian in Eq. (1) or in Eq. (8). The Hamiltonian *breaks* time-reversal symmetry via the presence of the artificial gauge field $\theta_y=\mathcal{A}_y\eta_y I$, where $\mathcal{A}_y$ plays the role of the y component of a vector potential. In addition, the Hamiltonian breaks particle-hole and chiral symmetries and its insulating phases can be labeled as an integer Z topological invariant, under the Cartan A classification of topological insulators [47–49]. This integer Z corresponds to the charge-charge Chern number $C^{\rm chch}$, which reflects the total chirality of edge states. For rational magnetic fluxes $\alpha=p/q$, a new periodicity of $2\pi/(qa_y)$ arises in the bulk along the k_y direction, but all edge states that emerge in bulk gaps are chiral pairs with periodicity $2\pi/a_y$ along k_y.

When a color-flip field h_x is present, with color-orbit coupling $k_T=0$, the color operator J_x remains conserved and the chirality of the edge states is preserved. Furthermore, even when $k_T\neq 0$, the edges states remain chiral, because the color-orbit mixing operator $\theta_x=k_T\eta_x J_z$ is nonchiral. Therefore, either in the absence or presence of color-orbit coupling $k_T a_x$, edge states are always chiral. It is this chirality that provides protection against perfect backscattering that leads to Anderson localization.

To highlight this protection, we consider the local disorder Hamiltonian

$$\hat{H}_{\rm dis}=\sum_{\mathbf{r}cc'}\phi_c^\dagger(\mathbf{r})D_{cc'}(\mathbf{r})\phi_{c'}(\mathbf{r})=\sum_{\mathbf{r}}\mathbf{\Phi}^\dagger(\mathbf{r})D(\mathbf{r})\mathbf{\Phi}(\mathbf{r}), \quad (32)$$

where $\mathbf{\Phi}(\mathbf{r})$ is a three-color vector (spinor) with components $\phi_c(\mathbf{r})$, and $\xi_{cc'}(\mathbf{r})$ are the elements of the random local matrix $D(\mathbf{r})$ that allows color flips, that is, $D_{cc'}(\mathbf{r})$ is not necessarily a diagonal matrix in the color indices $\{c,c'\}$. Since the disorder Hamiltonian $\hat{H}_{\rm dis}$ is local, then scattering can only occur between edge states located at the same boundary. However, since edge states always emerge in chiral pairs, there is no perfect backscattering caused by $\hat{H}_{\rm dis}$ leading to reversal of momentum $k_y\to -k_y$ and reversal of the band velocities $\partial E(k_y)/\partial k_y\to -\partial E(-k_y)/\partial k_y$ of edge states located at the same boundary. This is the case even when color flips are allowed in the local disorder potential. Therefore, in the absence of perfect backscattering, Anderson localization does not occur and edge states are protected by their chirality.

To visualize this general protection, let us analyze the three specific examples presented in Figs. 4 and 6, as well as in Fig. 8. In the case of Fig. 4, the color-orbit coupling is $k_T a_x=0$ and J_x is conserved. This means that the eigenstates of J_x are also eigenstates of the Hamiltonian $\hat{H}$ defined in Eq. (1) of the main text. Therefore, it is convenient to rotate the states $\phi_c(\mathbf{r})$ or the vector $\mathbf{\Phi}(\mathbf{r})$ from the color basis labeled by $c=\{R,G,B\}$ along the z axis to the color basis along the x axis labeled by c_x. This can be achieved by the unitary rotation $U_y=e^{-i(\pi/2)J_y}$ about the y axis. In this case, the disorder Hamiltonian becomes

$$\hat{H}_{\rm dis}=\sum_{\mathbf{r}}\bar{\mathbf{\Phi}}^\dagger(\mathbf{r})\bar{D}(\mathbf{r})\bar{\mathbf{\Phi}}(\mathbf{r}), \quad (33)$$

where the color spinor $\bar{\mathbf{\Phi}}(\mathbf{r})=U_y\mathbf{\Phi}(\mathbf{r})$ with elements $\bar{\phi}_{c_x}(\mathbf{r})$ is now labeled by c_x and the disorder matrix

$$\bar{D}(\mathbf{r})=U_y D(\mathbf{r})U_y^\dagger \quad (34)$$

with elements $\bar{D}_{c_x c_x'}(\mathbf{r})$ is labeled by $\{c_x,c_x'\}$.

A close look at Fig. 4 shows that there is no backscattering between edge states in the same boundary, when the disorder potential does not involve color flips. However, there is no perfect backscattering between the edge states on the right (R) boundary or between the edge states on the left (L) boundary, even when color flips are allowed. The sequence of edge states appearing in Fig. 4, with energy determined by the dashed line at $\mu/t_y=-1.07$ and increasing momentum k_y, can be labeled as $(L,-k_1,\uparrow_x)$ and $(R,-k_2,0_x)$ for the edge states with negative momentum and $(L,+k_2,0_x)$ and $(R,+k_1,\uparrow_x)$ for the edge states with positive momentum. When color flips are allowed by a weak local disorder potential there is some backscattering between the states $(L,-k_1,\uparrow_x)$ and $(L,+k_2,0_x)$, as well as between the states $(R,-k_2,0_x)$ and $(R,+k_1,\uparrow_x)$. However, the backscattering is far from perfect as the momenta and band velocities are not matched to produce Anderson localization. The protection of these edge states to weak local disorder is provided by their chirality.

When the color-orbit coupling $k_T\neq 0$ and $h_x\neq 0$, J_x is not conserved, but a similar situation also occurs. In this case, it is more convenient to write the disorder potential in the basis of eigenstates of the first-quantization Hamiltonian matrix $\hat{H}(\hat{\mathbf{k}})$ in Eq. (8). Starting with the disorder Hamiltonian

$$\hat{H}_{\rm dis}=\sum_i |i\rangle D_i\langle i| \quad (35)$$

where $|i\rangle$ represents the color field operator at position $\mathbf{r}$, that is, $|i\rangle=\mathbf{\Phi}^\dagger(\mathbf{r})$ and $D_i=D(\mathbf{r})$, we can rewrite

$$\hat{H}_{\rm dis}=\sum_{\chi,\chi'}|\chi\rangle D_{\chi\chi'}\langle\chi'|, \quad (36)$$

in the basis of edge eigenstates $|\chi\rangle$ of $\hat{H}(\hat{\mathbf{k}})$, where $|\chi\rangle=|\lambda,k_y,n_\alpha\rangle$ represents edge states at the $\lambda=\{R,L\}$ boundary, with momentum k_y and band index n_α, while $D_{\chi\chi'}=\sum_i\langle\chi|i\rangle D_i\langle i|\chi'\rangle$. The eigenstate projection in the original

basis can be written as $\phi_\chi(i) = \langle i|\chi\rangle$. Since the disorder potential is local, scattering between edge states within the bulk gap occurs only in the same boundary, which means that $D_{\chi\chi'}$ is diagonal in λ.

From the energy spectrum in Fig. 6, the sequence of edge states, with energy determined by the dashed line at $\mu/t_y = -1.11$ and increasing momentum k_y, can be labeled as $(L, -k_1, n_1)$ and $(R, -k_2, n_2)$ for the edge states with negative momentum and $(L, +k_2, n_2)$ and $(R, +k_1, n_1)$ for the edge states with positive momentum. For weak local disorder there is some backscattering between the states $(L, -k_1, n_1)$ and $(L, +k_2, n_2)$, as well as between the states $(R, -k_2, n_2)$ and $(R, +k_1, n_1)$. However, the backscattering is far from perfect as the momenta and band velocities are not matched to produce Anderson localization. The protection of these edge states to weak local disorder is provided by their chirality.

The same type of analysis can be made for the energy spectrum in Fig. 8 and the corresponding edge states within the bulk gap, say for $\mu/t_y = -0.37$. For weak disorder there is some backscattering between edge states on the same boundary. However, again, backscattering is far from perfect as the momenta and band velocities are not matched to produce Anderson localization. Once more, the protection of these edge states to weak local disorder is provided by their chirality.

The conduction channels for all edge states are protected against color-dependent and color-independent disorder, meaning that the topological insulating phases are *strong* with respect to disorder. This robustness is a direct consequence of the chirality of the edge states. Having considered the case of disorder, which is an extrinsic property in optical lattices, we turn our attention to the robustness of color edge states with respect to SU(3)-symmetric interactions, which can potentially gap edge states and suppress their ability to conduct, as discussed next.

B. Robustness of edge states against interactions

Closed-shell fermionic systems ^{173}Yb and ^{87}Sr have SU(N)-symmetric interactions, with $N \leqslant 6$ or 10, respectively. By experimentally selecting only three internal states, SU(3) systems can be explored. We focus on SU(3), because $N = 3$ gives the simplest system that shows nontrivial values of the topological invariant $C^{\rm coco}$. The local SU(3)-symmetric interactions

$$\hat{H}_{\rm int} = g \sum_{\mathbf{r}} \sum_{c\neq c'} \hat{n}_c(\mathbf{r})\hat{n}_{c'}(\mathbf{r}) \tag{37}$$

involve only repulsive ($g > 0$) density-density channels. The density operators are $\hat{n}_c(\mathbf{r}) = \phi_c^\dagger(\mathbf{r})\phi_c(\mathbf{r})$.

It is very important to emphasize that by using orbital-Feshbach techniques it is possible to control the strength of the SU(N)-symmetric interactions in order to increase them and to study strongly interacting systems or to decrease them to zero to study noninteracting systems [50,51]. So next, we analyze the effects of weak interactions on edge states.

To study the robustness of edge states to SU(3)-symmetric interactions existent in ^{173}Yb and ^{87}Sr, it is more convenient to express Eq. (37) in terms of the creation and annihilation operators of the eigenstates of the matrix Hamiltonian $\hat{H}(\hat{\mathbf{k}})$ in Eq. (8), and write the interaction between edge states as [36]

$$\hat{H}_{\rm int} = g \sum_{\substack{\lambda,\{n_s\}\\ k_{y_1},k_{y_3},q_y}} \gamma(\lambda,\{n_s\})\Lambda_{12}(k_{y_1},q_y)\Lambda_{34}(k_{y_3},q_y), \tag{38}$$

where $\gamma(\lambda,\{n_s\}) = \gamma(\lambda,n_1,n_2,n_3,n_4)$ are the interactions between edge states on the same edge, while $\Lambda_{12}(k_{y_1},q_y) = f^\dagger_{\lambda,n_1}(k_{y_1})f_{\lambda,n_2}(k_{y_1}+q_y)$ and $\Lambda_{34}(k_{y_3},q_y) = f^\dagger_{\lambda,n_3}(k_{y_3})f_{\lambda,n_4}(k_{y_3}-q_y)$ reflect the action of fermionic operators. Here, $f^\dagger_{\lambda,n_s}(k_{y_s})$ represents the creation operator of a fermion at the λ edge, with band index n_s and momentum k_{y_s}. These interactions together with kinetic energies

$$\hat{H}_{\rm K} = \sum_{\lambda,n} \varepsilon_{\lambda,n}(k_y) f^\dagger_{\lambda,n}(k_y) f_{\lambda,n}(k_y) \tag{39}$$

describe interacting edge states within bulk band gaps. By making the transformation, $q_y \to -q$, $k_{y_1} \to k_y + q$ and $k_{y_3} \to k'_y - q$, the interaction Hamiltonian above can be written in terms of generalized *density* operators $\hat{\rho}_{\lambda,n_i,n_j}(q) = \sum_{k_y} f^\dagger_{\lambda,n_i}(k_y+q)f_{\lambda,n_j}(k_y)$ as follows:

$$\hat{H}_{\rm int} = \sum_{\lambda,\{n_s\}} \gamma(\lambda,n_i,n_j,n_k,n_\ell)\hat{\rho}_{\lambda,n_i,n_j}(q)\hat{\rho}_{\lambda,n_k,n_\ell}(-q), \tag{40}$$

where the generalized *density* operators satisfy

$$\hat{\rho}^\dagger_{\lambda,n_i,n_j}(q) = \hat{\rho}_{\lambda,n_j,n_i}(-q). \tag{41}$$

To understand the role of local SU(3)-symmetric interactions on edge states, we analyze first the simplest situation of a single pair of chiral edge states, which occurs at high color-flip fields $h_x/t_y \gg 1$, irrespective of whether $k_T a_x = 0$ or $k_T a_x \neq 0$ for $\alpha = 1/3$ and $t_x/t_y = 1$. Some examples of single chiral edge states also occur for $\alpha = 1/3$, $t_x/t_y = 1$, $k_T a_x = \pi/8$, and $h_x/t_y = 2$, where the Chern numbers are either $\mathcal{C}^{\rm chch} = +1$, $\mathcal{C}^{\rm coch} = +1$, and $\mathcal{C}^{\rm coco} = +1$, for filling factor $\nu = 1/3$, or $\mathcal{C}^{\rm chch} = +1$, $\mathcal{C}^{\rm coch} = -1$, and $\mathcal{C}^{\rm coco} = -1$, for filling factor $\nu = 8/3$. In phases with only one edge state on each boundary, there is also only one interaction parameter $\tilde{g} = g\gamma(1,1,1,1)$ corresponding to forward scattering. Such a situation is simple, as the single edge state is protected by its chirality. So weak interactions can at most shift the energy of edge states and renormalize the Fermi velocity, but they will not open up a gap. The phases with a single pair of chiral edge states are robust against weak SU(3)-symmetric interactions, that is, they are *strong* topological phases where no minigaps emerge in the edge state spectrum to change their ability to conduct.

The situation is more complex in phases where there are two or more pairs of chiral edge states as shown in Figs. 4, 6, 8, given that many coupling constants are nonzero. Since interactions are local, right (R) and left (L) edge states do not interact, and we can treat each boundary separately. Thus, we look at the two right (R) edge states of Figs. 4 and 6, and a similar analysis can be done for the two left (L) edge states.

To illustrate the complexity of local SU(3)-symmetric interactions, we look first at the case of Fig. 4, where $k_T a_x = 0$ and J_x is conserved at the independent particle level. We can focus again on an edge, say the right one, and label the

edge states on the right boundary as $n = 1$ for negative momentum and $n = 2$ for positive momentum, noting that they have different c_x color projections. For two edge states on the same boundary, the interaction parameters $\gamma(n_1, n_2, n_3, n_4) \equiv \gamma(n_1 n_2 n_3 n_4)$ can have in general 16 different values, since each n_j can take two values $\{1, 2\}$. Due to color projection (c_x) conservation, interaction terms with three identical band indices vanish, that is, $\gamma(1112) = \gamma(1121) = \gamma(1211) = \gamma(1222) = 0$ for the series starting with $n = 1$ and $\gamma(2221) = \gamma(2212) = \gamma(2122) = \gamma(2111) = 0$ for the series restarting with $n = 2$. However, the other terms are nonzero: $\gamma(1111) = 0.40$, $\gamma(1122) = 0.49$, $\gamma(1212) = -0.16$, and $\gamma(1221) = -0.16$ for the series starting with $n = 1$, and $\gamma(2222) = 0.33$, $\gamma(2211) = 0.49$, $\gamma(2121) = -0.16$, and $\gamma(2112) = -0.16$ for the series starting with $n = 2$. The first two terms in each series correspond to forward scattering, while the second two terms correspond to backward scattering. In this case the interaction Hamiltonian reduces to

$$\begin{aligned}\hat{H}_{\rm int} = {} & \gamma(1111)\sum_q \rho_{11}(q)\rho_{11}(-q) + \gamma(1122)\sum_q \rho_{11}(q)\rho_{22}(-q) + \gamma(1212)\sum_q \rho_{12}(q)\rho_{12}(-q) \\ & + \gamma(1221)\sum_q \rho_{12}(q)\rho_{21}(-q) + \gamma(2222)\sum_q \rho_{22}(q)\rho_{22}(-q) + \gamma(2211)\sum_q \rho_{22}(q)\rho_{11}(-q) \\ & + \gamma(2121)\sum_q \rho_{21}(q)\rho_{21}(-q) + \gamma(2112)\sum_q \rho_{21}(q)\rho_{12}(-q),\end{aligned}$$

which involves the processes illustrated in Fig. 10, where we linearized the band dispersions of the edge states around their respective Fermi momenta k_{F_1} and k_{F_2}. The small momentum transfer processes controlled by $\gamma(1111)$ and $\gamma(2222)$ are shown in the left and right panels of Fig. 10(a), respectively. These processes are not so important, as they can at most shift a little the energies of the edge states. The small momentum transfer processes controlled by $\gamma(1122)$ and $\gamma(2211)$ are illustrated in the left panel of Fig. 10(b), while the large momentum transfer processes $\gamma(1221)$ and $\gamma(2112)$ are illustrated in the right panel of Fig. 10(b). These forward and backward scattering processes are very important, and are mostly responsible for creating small energy gaps in the edge state spectrum. Large momentum transfer processes (Umklapp-like) controlled by $\gamma(2121)$ and $\gamma(1212)$ are shown in the left and right panels of Fig. 10(c), respectively. These last processes are important only when the momentum $2(k_1 + k_2)$ matches the lattice wave vector $2\pi/a_y$, and thus require a special matching condition.

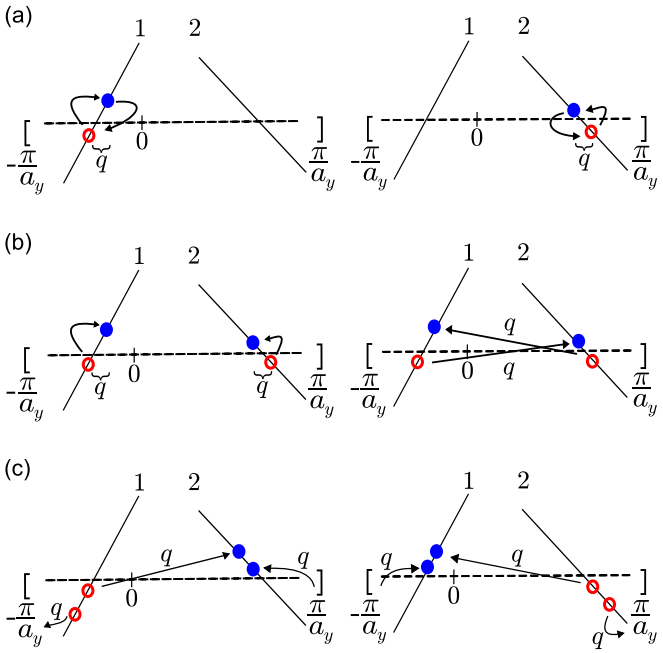

FIG. 10. Scattering processes originating from SU(3)-symmetric interactions between two edge states in a given boundary are shown. This situation corresponds to the example given in Fig. 4. Small momentum transfer (forward scattering) processes controlled by $\gamma(1111)$ and $\gamma(2222)$ are shown in the left and right panels of Fig. 10(a), respectively. Small momentum transfer (forward scattering) processes controlled by $\gamma(1122)$ and $\gamma(2211)$ are illustrated in the left panel of Fig. 10(b), while large momentum transfer (backward scattering) processes $\gamma(1221)$ and $\gamma(2112)$ are illustrated in the right panel of Fig. 10(b). Large momentum transfer processes (Umklapp-like) controlled by $\gamma(2121)$ and $\gamma(1212)$ are shown in the left and right panels of Fig. 10(c), respectively.

In the linear approximation, the kinetic energy of the edge states in the same boundary becomes

$$\begin{aligned}\hat{H}_{\rm K} = {} & \sum_{k_y}\left[\varepsilon\left(k_{F_1}\right) + v_{F_1}\left(k_y - k_{F_1}\right)\right] f_1^\dagger(k_y) f_1(k_y), \\ & + \sum_{k_y}\left[\varepsilon\left(k_{F_2}\right) + v_{F_2}\left(k_y - k_{F_2}\right)\right] f_2^\dagger(k_y) f_2(k_y),\end{aligned}$$

where the *velocities* are $v_{F_i} = \partial\varepsilon_i/\partial k_y|_{k_y = k_{F_i}}$. Using either mean-field theory, which is not reliable in one dimension, but can provide some insight, or bosonization techniques, we can show that these interactions may lead to the formation of a color density wave (CoDW), because backscattering is present. A small gap arises in the elementary excitation spectrum and the bosonic collective mode (CoDW) has linear dispersion. The analysis here follows closely the g-ology description [52] of one-dimensional nonchiral spinless fermions, where a charge-density wave emerges, using mean-field, renormalization-group, or bosonization methods. Similarly for nonchiral spin-1/2 fermions, mean-field, renormalization-group, and/or bosonization methods all show that one-dimensional Fermi gases are unstable towards charge-density wave, spin-density-wave, singlet-superconductivity, or triplet-superconductivity states, when interactions include backward (g_1) and forward (g_2) scattering processes [52].

Thus, the edge states in Fig. 4 are not robust with respect to SU(3)-symmetric interactions, and their chirality does not protect them from gapping out, since these edge states themselves are not eigenstates of an SU(3)-invariant independent particle Hamiltonian. This case then corresponds to a *weak* topological phase, where weak SU(3) interaction can lead to minigaps in the excitation spectrum of edge states and affect their ability to conduct. However, the effect of weak SU(3)-symmetric interactions is very small in the bulk. When $g \ll E_g$, where E_g is a bulk gap, the Chern numbers of the phase are unaffected, because the bulk gap cannot close and reopen. On the other hand, with the emergence of minigaps for edge states, the Hall conductances associated with a color component are no longer quantized.

For the edge states in Fig. 6, where the color-orbit coupling $k_T a_x \neq 0$, and J_x is not conserved, the SU(3)-symmetric interactions lead to 16 nonvanishing $\gamma(n_1 n_2 n_3 n_4)$ terms due to color mixing of different c_x projections. Now, a mixed-color density wave emerges at the edges, and the edge states develop a small gap. This is also a *weak* topological phase, that is, all edge states are gapped, and the corresponding color Hall conductances are affected, but the Chern numbers remain the same, provided that the SU(3)-symmetric interactions are weak in comparison to the bulk gap.

The analysis for topological phases with more than two edge states is quite elaborate. For the chemical potential shown in Fig. 8, there are three edge states in each boundary, and J_x is not conserved, since $k_T a_x \neq 0$. The SU(3)-symmetric interactions again induce a mixed-color density wave for two edge states at each boundary, but one of the edge states carrying chirality $+1$ remains ungapped, since the total chirality is conserved, that is, it cannot change without the closing and reappearance of a bulk gap. Weak SU(3)-symmetric interactions have a small effect on the bulk of the system, and all the Chern numbers remain robust. In this case, we have an *intermediate* topological phase, where two edge states develop a minigap, while the third one does not.

The main conclusion of this section is that edge states are robust to color-independent and color-dependent disorder in all topological phases. However, the robustness of edge states can be *strong*, *intermediate*, or *weak* with respect to SU(3)-symmetric interactions, depending on the emergence of minigaps that affect edge state conduction and associated color Hall conductances. The discussion above confirms, generalizes, and refines the conjecture that some edge states were potentially sensitive to SU(3)-symmetric interactions [36], and reveals that, even in such cases, the charge-charge, color-charge, and color-color Chern numbers remain robust to weak local perturbations, and do not change. This occurs, provided that weak local perturbations do not close bulk gaps with posterior reopenings that may change the topology of the ground-state wave function. Our results are SU(3) extensions of the conclusions of SU(2) spin-1/2 systems in honeycomb lattices [27,28], where minigaps in the spectrum of edge states may destroy the quantization of the spin-Hall conductance, but the spin Chern number, characteristic of the bulk bands, remains unchanged. Furthermore, our SU(3) examples provide extensions of general studies of the robustness of the spin-Chern number for SU(2) spin-1/2 systems with respect to disorder and time-reversal symmetry breaking [53], and its characterization as a property of the bulk, rather than as a property of the edge states.

IX. CLASSIFICATION OF TOPOLOGICAL COLOR INSULATORS

In Secs. III, IV, and V, we discussed the relation between the Hall conductances $\sigma_{yx}^{\rm chch}$, $\sigma_{yx}^{\rm coch}$ or $\sigma_{yx}^{\rm chco}$, and $\sigma_{yx}^{\rm coco}$, and the Chern numbers $\mathcal{C}^{\rm chch}$, $\mathcal{C}^{\rm coch}$ or $\mathcal{C}^{\rm chco}$, and $\mathcal{C}^{\rm coco}$. When color is conserved ($k_T a_x = 0$, $h_x \neq 0$, with conserved J_x), the corresponding Hall conductances for all insulating states are quantized and directly proportional to the Chern numbers $\mathcal{C}^{\rm chch}$, $\mathcal{C}^{\rm coch}$ or $\mathcal{C}^{\rm chco}$, and $\mathcal{C}^{\rm coco}$. In this case, all the insulating phases are characterized by quantized Hall conductances and by their associated Chern numbers, meaning that the Chern numbers can be obtained via the measurement of the quantized Hall conductances. When color is not conserved ($k_T a_x \neq 0$, $h_x \neq 0$, with nonconserved J_x), the charge-charge Hall conductance for the insulating states remains quantized, $\sigma_{yx}^{\rm chch} = (e^2/h)\mathcal{C}^{\rm chch}$, but the color-charge, charge-color, and color-color conductances are no longer proportional to corresponding Chern numbers, and thus no longer quantized. Nevertheless, the Chern numbers, which are a property of the ground-state wave function, can still be used to classify the insulating phases. However, measurements of color Hall conductances can no longer yield color Chern numbers that characterize the insulating phases. We concluded that to classify topological color insulators for SU(3) fermions, whether color is conserved or not, three topological invariants are necessary, $\mathcal{C}^{\rm chch}$, $\mathcal{C}^{\rm coch}$ or $\mathcal{C}^{\rm chco}$, and $\mathcal{C}^{\rm coco}$, unlike in the SU(2) spin-1/2 case, where only two are needed: $\mathcal{C}^{\rm chch}$, $\mathcal{C}^{\rm spch}$, or $\mathcal{C}^{\rm chsp}$.

In Sec. VIII, we provided a refinement of the classification of topological color insulators through an analysis of the robustness of edge state states with respect to disorder and interactions. We defined *strong* topological color insulators as systems where weak disorder and weak SU(3)-symmetric interactions do not affect the ability of all edge states to conduct. We defined *intermediate* topological color insulators as systems where weak disorder and weak SU(3)-symmetric interactions affect the ability of some, but not all, edge states to conduct. We defined *weak* topological color insulators as systems where weak disorder and weak SU(3)-symmetric interactions affect the ability of all edge states to conduct.

When charge and color are conserved, all Hall conductances are quantized and the corresponding Chern numbers can be extracted from Hall-conductance measurements. However, when color is not conserved or when edge states are not robust to disorder and/or interactions, the color Hall conductances are not quantized and their measurement cannot provide the color Chern numbers that characterize topological color insulators. This poses an experimental difficulty in measuring the relevant color Chern numbers. For such cases, it is necessary to identify bulk properties that relate to relevant color Chern numbers. For the quantum Hall effect, the Streda formula [54] connects the total density of states and filling factors to the magnetic flux and the charge-charge Chern number. This relation allows for the extraction of charge-charge Chern numbers from bulk measurements of filling factors or compressibility without the need to measure the

charge-charge Hall conductance. Thus, we conjecture that a color generalization of the Streda formula may allow for the extraction of color Chern numbers via bulk measurements of color-dependent filling factors or color-dependent compressibilities. The derivation of such relations is an important outlook for the measurement of color Chern numbers and, thus, for the experimental characterization of topological color insulators, whenever color Hall conductances are not quantized.

X. CONCLUSIONS

We investigated the quantum Hall response of SU(3) fermions and analyzed the charge-charge, color-charge, charge-color, and color-color Hall conductances. When color projection was conserved, we related color-Hall conductances to corresponding Chern numbers obtained from the Chern matrix. In this case, we found that measurements of color-Hall conductances can be used to extract color Chern numbers and reveal the topological nature of color-insulating phases. Even when color-Hall conductances are not quantized, we showed that color Chern numbers, which are properties of the ground-state wave function, can always be used to classify the topological insulating states. However, measurements of color-Hall conductances can no longer reveal the color Chern numbers, when color is not conserved. We showed that three topological invariants are necessary to classify topological color insulators: charge-charge, color-charge or charge-color, and color-color Chern numbers. Lastly, we refined this classification by analyzing the effects of disorder and SU(3)-symmetric interactions on the ability of edge states to conduct, and identified *weak*, *intermediate*, and *strong* topological color insulators. An important outlook is the identification of bulk measurements that may allow for the extraction of color Chern numbers, even in cases where the color-Hall conductances are not quantized. Such measurements are possible if conjectured relations between the color-dependent density of states or color-dependent filling factors as a function of the magnetic flux and color Chern numbers are derived.

[1] T. Fukuhara, Y. Takasu, M. Kumakura, and Y. Takahashi, Degenerate Fermi Gases of Ytterbium, Phys. Rev. Lett. **98**, 030401 (2007).

[2] M. A. Cazalilla, A. F. Ho, and M. Ueda, Ultracold gases of ytterbium: ferromagnetism and Mott states in an SU(6) Fermi system, New J. Phys. **11**, 103033 (2009).

[3] S. Taie, Y. Takasu, S. Sugawa, R. Yamazaki, T. Tsujimoto, R. Murakami, and Y. Takahashi, Realization of a SU(2)×SU(6) System of Fermions in a Cold Atomic Gas, Phys. Rev. Lett. **105**, 190401 (2010).

[4] S. Taie, R. Yamazaki, S. Sugawa, and Y. Takahashi, An SU(6) Mott insulator of an atomic Fermi gas realized by large-spin Pomeranchuk cooling, Nat. Phys. **8**, 825 (2012).

[5] F. Scazza, C. Hofrichter, M. Höfer, P. C. De Groot, I. Bloch, and S. Fölling, Observation of two-orbital spin-exchange interactions with ultracold SU(N)-symmetric fermions, Nat. Phys. **10**, 779 (2014).

[6] G. Pagano, M. Mancini, G. Cappellini, P. Lombardi, F. Schäfer, H. Hu, X. J. Liu, J. Catani, C. Sias, M. Inguscio, and L. Fallani, A one-dimensional liquid of fermions with tunable spin, Nat. Phys. **10**, 198 (2014).

[7] C. Hofrichter, L. Riegger, F. Scazza, M. Höfer, D. R. Fernandes, I. Bloch, and S. Fölling, Direct Probing of the Mott Crossover in the SU(N) Fermi-Hubbard Model, Phys. Rev. X **6**, 021030 (2016).

[8] L. F. Livi, G. Cappellini, M. Diem, L. Franchi, C. Clivati, M. Frittelli, F. Levi, D. Calonico, J. Catani, M. Inguscio, and L. Fallani, Synthetic Dimensions and Spin-Orbit Coupling with an Optical Clock Transition, Phys. Rev. Lett. **117**, 220401 (2016).

[9] H. Ozawa, S. Taie, Y. Takasu, and Y. Takahashi, Antiferromagnetic Spin Correlation of SU (N) Fermi Gas in an Optical Superlattice, Phys. Rev. Lett. **121**, 225303 (2018).

[10] B. J. DeSalvo, M. Yan, P. G. Mickelson, Y. N. Martinez de Escobar, and T. C. Killian, Degenerate Fermi Gas of ^{87}Sr, Phys. Rev. Lett. **105**, 030402 (2010).

[11] M. K. Tey, S. Stellmer, R. Grimm, and F. Schreck, Double-degenerate Bose-Fermi mixture of strontium, Phys. Rev. A **82**, 011608(R) (2010).

[12] S. Stellmer, R. Grimm, and F. Schreck, Detection and manipulation of nuclear spin states in fermionic strontium, Phys. Rev. A **84**, 043611 (2011).

[13] S. Stellmer, F. Schreck, and T. C. Killian, Degenerate quantum gases of strontium, in *Annual Review of Cold Atoms and Molecules*, edited by K. W. Madison, K. Bongs, L. D. Carr, A. M. Rey, and H. Zhai (World Scientific, Singapore, 2014), Chap. 1, pp. 1–80.

[14] M. Aidelsburger, M. Atala, M. Lohse, J. T. Barreiro, B. Paredes, and I. Bloch, Realization of the Hofstadter Hamiltonian with Ultracold Atoms in Optical Lattices, Phys. Rev. Lett. **111**, 185301 (2013).

[15] H. Miyake, G. A. Siviloglou, C. J. Kennedy, W. C. Burton, and W. Ketterle, Realizing the Harper Hamiltonian with Laser-Assisted Tunneling in Optical Lattices, Phys. Rev. Lett. **111**, 185302 (2013).

[16] G. Jotzu, M. Messer, R. Desbuquois, M. Lebrat, T. Uehlinger, D. Greif, and T. Esslinger, Experimental realization of the topological Haldane model with ultracold fermions, Nature (London) **515**, 237 (2014).

[17] M. Aidelsburger, M. Lohse, C. Schweizer, M. Atala, J. T. Barreiro, S. Nascimbene, N. R. Cooper, I. Bloch, and N. Goldman, Measuring the Chern number of Hofstadter bands with ultracold bosonic atoms, Nat. Phys. **11**, 162 (2015).

[18] E. Zhao, N. Bray-Ali, C. J. Williams, I. B. Spielman, and I. I. Satija, Chern numbers hiding in time-of-flight images, Phys. Rev. A **84**, 063629 (2011).

[19] H. M. Price and N. R. Cooper, Mapping the Berry curvature from semiclassical dynamics in optical lattices, Phys. Rev. A **85**, 033620 (2012).

[20] A. Dauphin and N. Goldman, Extracting the Chern Number from the Dynamics of a Fermi Gas: Implementing a Quantum Hall Bar for Cold Atoms, Phys. Rev. Lett. **111**, 135302 (2013).

[21] D. J. Thouless, M. Kohmoto, M. P. Nightingale, and M. den Nijs, Quantized Hall Conductance in a Two-Dimensional Periodic Potential, Phys. Rev. Lett. **49**, 405 (1982).
[22] M. Kohmoto, Topological invariant and the quantization of the Hall conductance, Ann. Phys. (NY) **160**, 343 (1985).
[23] Y. Hatsugai, Chern Number and Edge States in the Integer Quantum Hall Effect, Phys. Rev. Lett. **71**, 3697 (1993).
[24] Y. Hatsugai, Topological aspects of the quantum Hall effect, J. Phys.: Condens. Matter **9**, 2507 (1997).
[25] F. D. M. Haldane, Model for a Quantum Hall Effect Without Landau Levels: Condensed-Matter Realization of the Parity Anomaly, Phys. Rev. Lett. **61**, 2015 (1988).
[26] C. L. Kane and E. J. Mele, Z_2 Topological Order and the Quantum Spin Hall Effect, Phys. Rev. Lett. **95**, 146802 (2005).
[27] Y. Yang, Z. Xu, L. Sheng, B. Wang, D. Y. Xing, and D. N. Sheng, Time-Reversal-Symmetry-Broken Quantum Spin Hall Effect, Phys. Rev. Lett. **107**, 066602 (2011).
[28] W. Beugeling, N. Goldman, and C. Morais Smith, Topological phases in a two-dimensional lattice: Magnetic field versus spin-orbit coupling, Phys. Rev. B **86**, 075118 (2012).
[29] M. H. Yau and C. A. R. Sá de Melo, Topological Color-Hall Insulators: SU(3) Fermions in Optical Lattices, arXiv:1904.12791.
[30] M. H. Yau and C. A. R. Sá de Melo, SU(3) vs. SU(2) fermions in optical lattices: Color-Hall vs. spin-Hall topological insulators, Europhys. Lett. **135**, 16001 (2021).
[31] Y. J. Lin, K. Jimenez-Garcia, and I. B. Spielman, Spin-orbit coupled Bose-Einstein condensates, Nature (London) **471**, 83 (2011).
[32] N. Goldman, I. Satija, P. Nikolic, A. Bermudez, M. A. Martin-Delgado, M. Lewenstein, and I. B. Spielman, Realistic Time-Reversal Invariant Topological Insulators with Neutral Atoms, Phys. Rev. Lett. **105**, 255302 (2010).
[33] J. Shi, P. Zhang, D. Xiao, and Q. Niu, Proper Definition of Spin Current in Spin-Orbit Coupled Systems, Phys. Rev. Lett. **96**, 076604 (2006).
[34] P. Zhang, Z. Wang, J. Shi, D. Xiao, and Q. Niu, Theory of conserved spin current and its application to a two-dimensional hole gas, Phys. Rev. B **77**, 075304 (2008).
[35] R. Kubo, Statistical-mechanical theory of irreversible processes. I. General theory and simple applications to magnetic and conduction problems, J. Phys. Soc. Jpn. **12**, 570 (1957).
[36] M. H. Yau and C. A. R. Sá de Melo, Eigenspectrum, Chern numbers and phase diagrams of ultracold color-orbit-coupled SU(3) fermions in optical lattices, Phys. Rev. A **103**, 043302 (2021).
[37] D. M. Kurkcuoglu and C. A. R. Sá de Melo, Creating spin-one fermions in the presence of artificial spin-orbit fields: Emergent spinor physics and spectroscopic properties, J. Low Temp. Phys. **191**, 174 (2018).
[38] D. M. Kurkcuoglu and C. A. R. Sá de Melo, Color superfluidity of neutral ultracold fermions in the presence of color-flip and color-orbit fields, Phys. Rev. A **97**, 023632 (2018).
[39] Q. Niu, D. J. Thouless, and Y. S. Wu, Quantized Hall conductance as a topological invariant, Phys. Rev. B **31**, 3372 (1985).
[40] J. E. Avron and R. Seiler, Quantization of the Hall Conductance for General, Multiparticle Schrodinger Hamiltonians, Phys. Rev. Lett. **54**, 259 (1985).
[41] D. N. Sheng, L. Balents, and Z. Wang, Phase Diagram for Quantum Hall Bilayers at $\nu = 1$, Phys. Rev. Lett. **91**, 116802 (2003).
[42] D. N. Sheng, Z. Y. Weng, L. Sheng, and F. D. M. Haldane, Quantum Spin-Hall Effect and Topologically Invariant Chern Numbers, Phys. Rev. Lett. **97**, 036808 (2006).
[43] J. Billy, V. Josse, Z. Zuo, A. Bernard, B. Hambrecht, P. Lugan, D. Clément, L. Sanchez-Palencia, P. Bouyer, and A. Aspect, Direct observation of Anderson localization of matter waves in a controlled disorder, Nature (London) **453**, 891 (2008).
[44] Y. Yue, C. A. R. Sá de Melo, and I. B. Spielman, Enhanced transport of spin-orbit-coupled Bose gases in disordered potentials, Phys. Rev. A **102**, 033325 (2020).
[45] G. Roati, C. D'Errico, L. Fallani, M. Fattori, C. Fort, M. Zaccanti, G. Modugno, M. Modugno, and M. Inguscio, Anderson localization of a non-interacting Bose-Einstein condensate, Nature (London) **453**, 895 (2008).
[46] L. Han and C. A. R. Sá de Melo, Evolution from Bardeen-Cooper-Schrieffer to Bose-Einstein condensate superfluidity in the presence of disorder, New J. Phys. **13**, 055012 (2011).
[47] A. Altland and M. R. Zirnbauer, Nonstandard symmetry classes in mesoscopic normal-superconducting hybrid structures, Phys. Rev. B **55**, 1142 (1997).
[48] S. Ryu, A. P. Schnyder, A. Furusaki, and A. W. W. Ludwig, Topological insulators and superconductors: Tenfoldway and dimensional hierarchy, New J. Phys. **12**, 065010 (2010)
[49] C.-K. Chiu, J. C. Y. Teo, A. P. Schnyder, and S. Ryu, Classification of topological quantum matter with symmetries, Rev. Mod. Phys. **88**, 035005 (2016).
[50] G. Pagano, M. Mancini, G. Cappellini, L. Livi, C. Sias, J. Catani, M. Inguscio, and L. Fallani, Strongly Interacting Gas of Two-Electron Fermions at an Orbital Feshbach Resonance, Phys. Rev. Lett. **115**, 265301 (2015).
[51] M. Höfer, L. Riegger, F. Scazza, C. Hofrichter, D. R. Fernandes, M. M. Parish, J. Levinsen, I. Bloch, and S. Fölling, Observation of an Orbital Interaction-Induced Feshbach Resonance in ^{173}Yb, Phys. Rev. Lett. **115**, 265302 (2015).
[52] J. Solyom, The Fermi gas model of one-dimensional conductors, Adv. Phys. **28**, 201 (1979).
[53] E. Prodan, Robustness of the spin-Chern number, Phys. Rev. B **80**, 125327 (2009).
[54] P. Streda, Theory of quantised Hall conductivity in two dimensions, J. Phys. C: Solid State Phys. **15**, L717 (1982).